© 2016. Published by The Company of Biologists Ltd | Development (2016) 143, 4441-4451 doi:10.1242/dev.140129

RESEARCH ARTICLE

Syndecan 4 controls lymphatic vasculature remodeling during mouse embryonic development

Yingdi Wang[1], Nicolas Baeyens[1,*], Federico Corti[1], Keiichiro Tanaka[1], Jennifer S. Fang[1], Jiasheng Zhang[1], Yu Jin[1], Brian Coon[1], Karen K. Hirschi[1,2], Martin A. Schwartz[1,3,4] and Michael Simons[1,3,‡]

ABSTRACT

The role of fluid shear stress in vasculature development and remodeling is well appreciated. However, the mechanisms regulating these effects remain elusive. We show that abnormal flow sensing in lymphatic endothelial cells (LECs) caused by *Sdc4* or *Pecam1* deletion in mice results in impaired lymphatic vessel remodeling, including abnormal valve morphogenesis. Ablation of either gene leads to the formation of irregular, enlarged and excessively branched lymphatic vessels. In both cases, lymphatic valve-forming endothelial cells are randomly oriented, resulting in the formation of abnormal valves. These abnormalities are much more pronounced in *Sdc4*$^{-/-}$; *Pecam1*$^{-/-}$ double-knockout mice, which develop severe edema. *In vitro*, *SDC4* knockdown human LECs fail to align under flow and exhibit high expression of the planar cell polarity protein VANGL2. Reducing VANGL2 levels in *SDC4* knockdown LECs restores their alignment under flow, while VANGL2 overexpression in wild-type LECs mimics the flow alignment abnormalities seen in *SDC4* knockdown LECs. SDC4 thus controls flow-induced LEC polarization via regulation of VANGL2 expression.

KEY WORDS: Syndecan 4, Lymphatic remodeling, Embryonic development

INTRODUCTION

Tissue remodeling is an important process during organogenesis. In the vascular system, fluid flow plays a crucial role in the morphogenesis of both blood and lymphatic vasculature in a manner that is still poorly understood. Lymphatic vessels constitute a distinct vascular network that takes up interstitial fluid (lymph) and returns it to systemic circulation. The effective unidirectional transport of the lymphatic fluid requires the formation of lymphatic intraluminal valves (hereafter referred to as lymphatic valves) that prevent backflow of lymph. A previous study has established that initiation of lymphatic fluid flow is required for the development of lymphatic valves, a process that involves the transcription factors Prox1 and FoxC2 (Sabine et al., 2012). Flow is also required for lymphatic fate maintenance (Chen et al., 2012), lymphatic collecting vessel maturation (Sweet et al., 2015) and lymphatic vessel stabilization (Sabine et al., 2015). Despite these data pointing to the role of fluid flow in lymphatic vasculature development, the molecular mechanisms involved in mechanotransduction in the lymphatic endothelium have not been established.

In blood endothelial cells (BECs), fluid shear stress (FSS) signaling is mediated, in part, by a junctional mechanosensory complex that includes platelet and endothelial cell adhesion molecule 1 (PECAM1), vascular endothelial cell cadherin [VE-cadherin; also known as cadherin 5 (CDH5)] and vascular endothelial growth factor receptor 2 (VEGFR2; also known as KDR) (Tzima et al., 2005). Recently, VEGFR3 (FLT4) has been identified as a new component of this mechanosensory complex (Coon et al., 2015). Interestingly, the levels of VEGFR3 expression regulate the sensitivity of endothelial cells (ECs) to FSS, with higher expression leading to greater sensitivity to flow signal (Baeyens et al., 2015).

In addition to the mechanosensory complex described above, syndecan 4 has emerged as another regulator of FSS-induced EC alignment (Baeyens et al., 2014). In addition to flow, syndecan 4 also has the ability to respond to directly applied mechanical tension (Bellin et al., 2009). However, the molecular mechanism underlying the syndecan 4-dependent shear stress response is unknown. Syndecan 4 is a transmembrane heparin sulfate proteoglycan that contributes to a number of cellular signaling events (Elfenbein and Simons, 2013). It has been implicated in the regulation of fibroblast growth factor signaling in the endothelium (Elfenbein et al., 2012; Horowitz et al., 2002), mechanical stress-induced activation of the calcineurin-NFAT pathway in cardiomyocytes (Finsen et al., 2011), and in modulation of the Wnt/β-catenin pathway in *Xenopus* via interaction with the LRP6 receptor (Astudillo et al., 2014). Syndecan 4 also regulates the Wnt/planar cell polarity (PCP) pathway during convergent extension (Muñoz et al., 2006), and induces clathrin-mediated endocytosis in PCP signaling (Ohkawara et al., 2011). In mouse, syndecan 4 (Sdc4) has been shown to interact genetically with the core PCP protein vang-like 2 (Vangl2), through which it regulates neural tube closure, wound healing and stereocilia orientation in sensory hair cells (Escobedo et al., 2013).

Given this involvement of SDC4 and PECAM1 in mechanotransduction, we set out to study the role of these proteins in lymphatic vasculature development. We find that deletion of either *Sdc4* or *Pecam1* in mice results in abnormal lymphatic vessel remodeling and, in particular, abnormal lymphatic valve formation due to the failure of lymphatic valve-forming ECs to properly align under flow. Deletion of both genes resulted in more profound abnormalities than caused by deletion of either gene alone. Finally, in the case of *Sdc4* deletion, these effects were mediated by an abnormal flow-induced increase in Vangl2 levels.

[1]Yale Cardiovascular Research Center, Department of Internal Medicine, Yale University School of Medicine, New Haven, CT 06511, USA. [2]Yale Stem Cell Center, Yale University School of Medicine, New Haven, CT 06520, USA. [3]Department of Cell Biology, Yale University School of Medicine, New Haven, CT 06520, USA. [4]Department of Biomedical Engineering, Yale University School of Medicine, New Haven, CT 06520, USA.
*Present address: Wellcome Trust Centre for Cell-Matrix Research, Faculty of Biology, Medicine and Health, The University of Manchester, Manchester M13 9PT, UK.

‡Author for correspondence (michael.simons@yale.edu)

M.S., 0000-0003-0348-7734

Received 20 May 2016; Accepted 19 October 2016

Development (2016) 143, 4441-4451 doi:10.1242/dev.140129

RESULTS

Lymphatic vessels show remodeling defects in *Sdc4*$^{-/-}$ mice

To study the function of Sdc4 in lymphatic vasculature formation, we used the development of mesenteric vessels as a model. In control mice, small-diameter, cord-like lymphatic endothelial structures (Prox1^{+}, Vegfr3^{+}, VE-cadherin^{+}) are present by embryonic day (E) 14.5 (Fig. S1A, white arrow). The lymphatic endothelial cells (LECs) in these vessels extend fine cellular processes in order to connect to each other (Fig. S1A, yellow arrow). By E15.5, larger diameter lymphatic tubular structures are formed (Fig. S1A, arrow) and a complex, honeycombed primary lymphatic plexus (Prox1^{+}, Vegfr3^{+}) has developed by E16.5 (Fig. S1B). This primary lymphatic plexus is then remodeled into a complete lymphatic vascular network including capillaries and collecting lymphatic vessels (Fig. 1A,B).

In *Sdc4*$^{-/-}$ mice, the development of mesenteric lymphatic vessels is similar to that of the control from E14.5 through E16.5 (Fig. S1A,B). However, abnormal lymphatic vessels are observed in the mutants at later embryonic stages (Fig. 1C,D). At E18.5, instead of forming a hierarchal vascular network (Fig. 1A,B), mesenteric lymphatic vessels in *Sdc4* nulls tend to form a vascular plexus with multiple branches (Fig. 1C). Compared with littermate controls, cell-cell junctions in *Sdc4*$^{-/-}$ mice are less linear and show numerous protrusions, exhibiting a wavy appearance (Fig. S1C). Moreover, enlarged, irregular lymphatic vessels are frequently seen in *Sdc4* nulls (Fig. 1D).

To determine the cause of the increased lymphatic vessel diameter, we examined the cell cycle distribution of LECs and BECs in the mutants using fluorescence-activated cell sorting (FACS) (Fig. S2A,B). The number of LECs in the S/G2/M phases of the cell cycle was increased in *Sdc4*$^{-/-}$ mice compared with controls (Fig. S2A), suggesting increased proliferation. Importantly, this was not seen in BECs in *Sdc4* nulls (Fig. S2B). These data are consistent with increased lymphatic but not blood vessel diameter in *Sdc4*$^{-/-}$ mice.

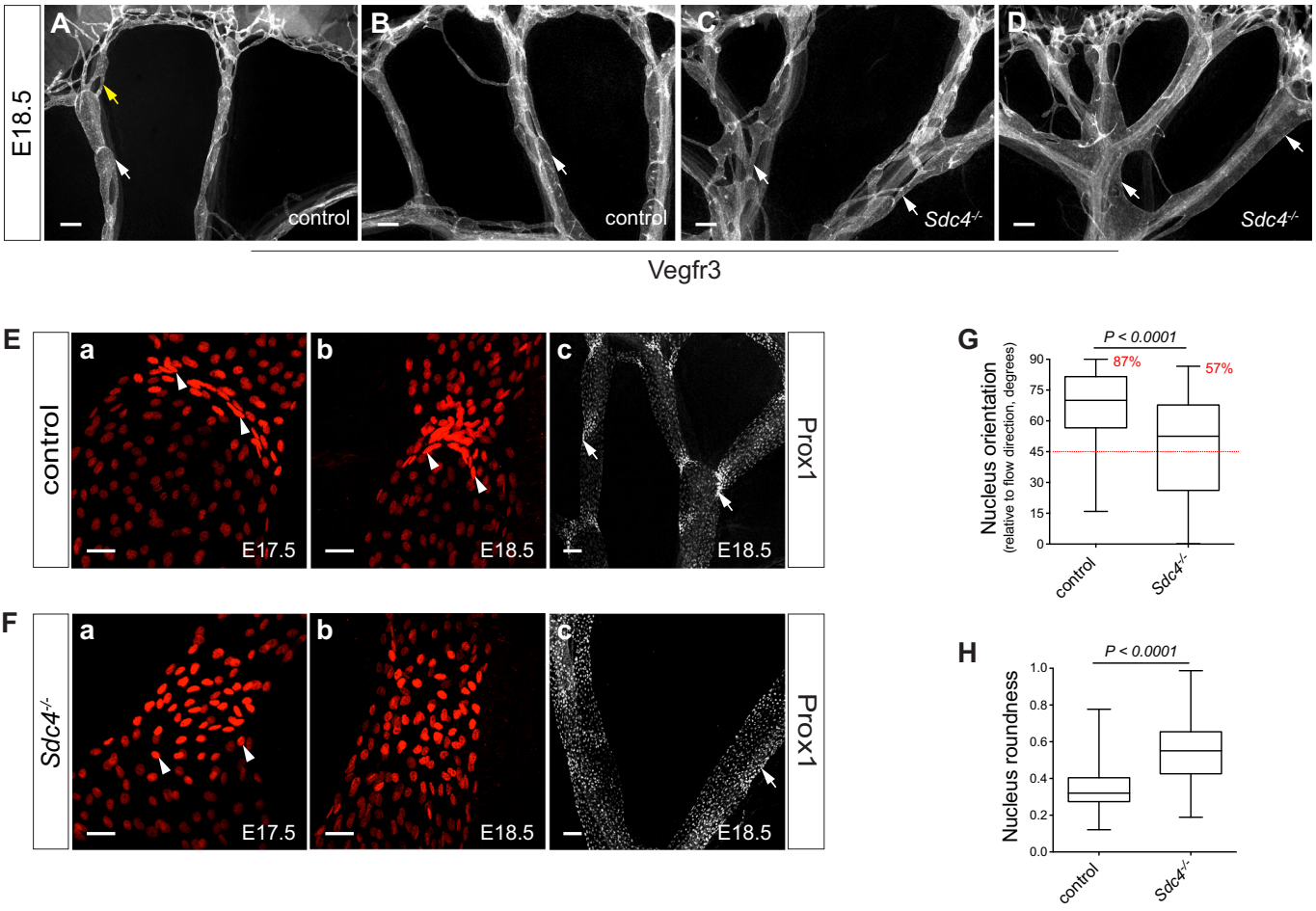

Fig. 1. Lymphatic vessels show remodeling defects in *Sdc4*$^{-/-}$ mice during late embryonic development. (A-D) Whole-mount immunofluorescence staining for Vegfr3, showing a hierarchal lymphatic vascular network in the mesentery of control mice at E18.5 (A,B); yellow arrow, capillaries; white arrows, lymphatic collecting vessels. In *Sdc4* nulls, by contrast, lymphatic vessels are abnormally branched and tend to form a vascular plexus (C, arrows). Enlarged lymphatic vessels were also seen in *Sdc4*$^{-/-}$ mice (D, arrows). (E) Prox1^{high} lymphatic valve-forming ECs reorient perpendicular to flow direction at E17.5 in control animals. The nuclei of valve-forming cells are highly elongated and are tightly packed (a, arrowheads). At E18.5, valve-forming cells reorganize again and form mature lymphatic valves containing two leaflets (b, arrowheads). Prox1^{high} valve-forming cells are concentrated in valve areas in the control (c, arrows). (F) The nuclei of Prox1^{high} valve-forming cells are rounded (a, arrowheads), randomly oriented and loosely arranged in *Sdc4*$^{-/-}$ mice at E17.5. Nuclei of similar morphology and organization were also seen in the mutants at E18.5 (b). Some of the Prox1^{high} valve-forming cells in *Sdc4*$^{-/-}$ embryos do not reorient, and remain parallel to the longitudinal axis of lymphatic vessels (c, arrow). (G) Nuclear orientation of Prox1^{high} cells in E17.5 mesenteric lymphatic vessels of control and *Sdc4*$^{-/-}$ mice (n=5). The percentage of nuclei reoriented >45° relative to flow direction is indicated. Mann–Whitney test. (H) Quantification of nuclear shape (roundness) of Prox1^{high} cells in E17.5 mesenteric lymphatic vessels (n=5). Mann–Whitney test. Scale bars: 200 µm in A-D; 30 µm in Ea,b,Fa,b; 100 µm in Ec,Fc.

Development (2016) 143, 4441-4451 doi:10.1242/dev.140129

Prox1^{high} lymphatic valve-forming ECs in *Sdc4* nulls are abnormally oriented

Given these remodeling abnormalities, we set out to investigate the development of lymphatic valves, an important event during lymphatic vasculature remodeling. In control mice, lymphatic valves start to develop in mesenteric lymphatic vessels at E16.5 (Sabine et al., 2012; Tatin et al., 2013). This is also the time when flow begins (Sabine et al., 2012). In agreement with previous reports (Sabine et al., 2012; Tatin et al., 2013), the development of lymphatic valves in control mice begins by the formation of clusters of Prox1^{high} lymphatic valve-forming ECs that are initially aligned along the longitudinal axis of lymphatic vessels (Fig. S1D). Valve-forming cells subsequently reorient 90° and become perpendicular to the direction of flow (Fig. 1Ea). During this reorientation process, the nuclei of Prox1^{high} valve-forming cells show morphological and organizational changes, becoming highly elongated and tightly packed (Fig. 1Ea). Furthermore, nuclear morphology and orientation are highly correlated with cell morphology and cell orientation (Fig. S3). By contrast, in *Sdc4*$^{-/-}$ mice, the nuclei of Prox1^{high} cells are rounded, randomly oriented and loosely organized (Fig. 1Fa).

Since it is more accurate to measure nuclear rather than cell orientation, we assessed valve-forming cell orientation by measuring the angle of nuclei relative to the flow direction (Fig. 1G). In control mice, the majority of valve-forming cells (87%) are oriented ≥45° relative to flow direction at E17.5 (Fig. 1G). In *Sdc4* nulls, even though the formation of lymphatic valves begins normally (Fig. S1D), only 57% of the valve-forming cells are oriented ≥45° (Fig. 1G). Nearly half of the valve-forming cells (43%) in *Sdc4* nulls are arranged within 45° relative to flow direction (Fig. 1G).

The morphology of Prox1^{high} LECs was examined by measuring the roundness of the nuclei (Fig. 1H). In agreement with immunostaining results at E17.5 (Fig. 1Ea,Fa), Prox1^{high} valve-forming cells in *Sdc4* nulls are less elongated than in controls (Fig. 1H). Moreover, Prox1^{high} valve-forming cells in *Sdc4* nulls are loosely organized and form a wide band of cells (Fig. 1Fa,b), whereas they are tightly packed in control embryos (Fig. 1Ea,b). At E18.5, valve-forming cells in control animals reorient again to form mature lymphatic valves that have two leaflets (Fig. 1Eb), whereas in *Sdc4* nulls the Prox1^{high} LECs exhibit a similar organization as at E17.5 (Fig. 1Fb). Also, some of the Prox1^{high} cells in *Sdc4* nulls do not reorient and remain parallel to the flow direction along the lymphatic vessel wall (Fig. 1Fc). By contrast, Prox1^{high} LECs in control mice are concentrated in valve-forming areas (Fig. 1Ec).

We further investigated cell alignment by examining actin filament remodeling and alignment in lymphatic vessels. Phalloidin labeling showed that in control lymphatics the actin filaments are remodeled into long, fine fibers that are aligned in the direction of flow (Fig. 2A). By contrast, in *Sdc4*$^{-/-}$ mice the actin fibers of LECs have a short, thick appearance and are randomly organized (Fig. 2B).

To examine whether the abnormal reorientation of lymphatic valve-forming cells in *Sdc4*$^{-/-}$ mice compromises lymphatic valve development, we quantified the formation of valves. In control E18.5 animals, the majority (88.5%) of lymphatic valves are mature V-shaped valves (Fig. 2C), although there is a small minority (11.5%) of immature valves with a ring-shaped morphology (Fig. 2F). By contrast, in *Sdc4* nulls, mature lymphatic valves are rarely seen (9.3%) at E18.5 (Fig. 2F). The majority of lymphatic valves in the mutants retain the ring-shaped appearance of immature valves (26%) (Fig. 2D,F) or appear highly abnormal (64.7%) with Prox1^{high} valve-forming cells either randomly oriented or aligned parallel to the flow direction (Fig. 2E,F).

Together, these data show that Sdc4 is important in regulating Prox1^{high} lymphatic valve-forming EC reorientation and lymphatic valve formation during embryonic development. Although *Sdc4* null mice can survive to adulthood, abnormal lymphatic valves were also observed in dermal lymphatic vessels of *Sdc4*$^{-/-}$ adults (Fig. S4C,D).

Abnormal lymphatic vessel development in *Pecam1* null mice

To establish whether abnormalities in lymphatic development noted in *Sdc4*$^{-/-}$ mice were due to abnormal shear stress sensing or other features of Sdc4 biology, we examined lymphatic vessel morphogenesis in *Pecam1* null mice that have a flow sensing defect. As in *Sdc4*$^{-/-}$, the *Pecam1*$^{-/-}$ mice did not display any lymphatic abnormalities during early stages of embryonic development (E14.5 to E16.5, Fig. S5A-F). However, by E18.5, unlike littermate controls (Fig. 3A), these mutants develop irregular (Fig. 3B, Fig. S6B), enlarged (Fig. 3C, Fig. S6C,G,H) and abnormally branched (Fig. 3D, Fig. S6C,D) mesenteric lymphatic vessels.

FACS analysis of LECs and BECs isolated from mesenteries of E18.5 embryos demonstrated a decrease in the number of cells in the S/G2/M phases of the cell cycle in *Pecam1*$^{-/-}$ mice and increased numbers of cells at G1 phase (Fig. S2C,D). Thus, increased cell proliferation does not account for the increased vessel diameter seen in these animals.

Prox1^{high} valve-forming cells in *Pecam1* nulls were less elongated, randomly oriented and loosely organized (Fig. 3Fa,b,G, Fig. S6I) compared with controls (Fig. 3Ea,b,G). Moreover, some of the valve-forming cells in *Pecam1* nulls fail to reorient and are aligned along the lymphatic vessel wall (Fig. S6J). Prox1^{high} LECs that are not concentrated in valve-forming areas are often seen in *Pecam1* nulls (Fig. 3Fc).

Unlike in control mice, where the majority of Prox1^{high} valve-forming cells are oriented perpendicular to the flow direction at E17.5 (Fig. 3Ea,c), with the majority (85%) of nuclei aligning at ≥45° relative to the flow direction (Fig. 3H), in *Pecam1*$^{-/-}$ mice a much smaller proportion of valve-forming cells (52%) exhibited this degree of nuclear orientation (Fig. 3H). In agreement with these findings, actin filaments of LECs were not aligned with flow in *Pecam1*$^{-/-}$ mice (Fig. 4A,B).

The abnormal reorientation of valve-forming cells in *Pecam1* nulls results in significantly reduced formation of mature lymphatic valves and the development of immature and abnormal valves at E18.5 (Fig. 4C-E, Fig. S6K-N).

Sdc4$^{-/-}$; *Pecam1*$^{-/-}$ double-knockout mice develop a severe lymphatic phenotype

To test a genetic interaction between Sdc4 and Pecam1 with regard to lymphatic vasculature development, we generated *Sdc4*$^{-/-}$; *Pecam1*$^{-/-}$ double-knockout mice. Examination of the mesenteric lymphatic vessels revealed much more extensive abnormalities, including irregular morphology, increased diameter and abnormal branching (Fig. 5A), in *Sdc4*$^{-/-}$; *Pecam1*$^{-/-}$ animals than in mice with a single gene deletion. Blood-filled jugular lymph sac was observed in *Sdc4*$^{-/-}$; *Pecam1*$^{-/-}$ embryos at E15.5 (Fig. S7). At E15.5, 8% of the *Sdc4*$^{-/-}$; *Pecam1*$^{-/-}$ embryos were lethal, 77% exhibited blood-filled lymphatic structures and/or edema, while 15% appeared normal. Those *Sdc4*$^{-/-}$; *Pecam1*$^{-/-}$ mice that survived to adulthood appeared normal and fertile.

Mural cell coverage in lymphatic vessels was somewhat increased in both *Sdc4*$^{-/-}$ and *Pecam1*$^{-/-}$ embryos compared with controls

Development (2016) 143, 4441-4451 doi:10.1242/dev.140129

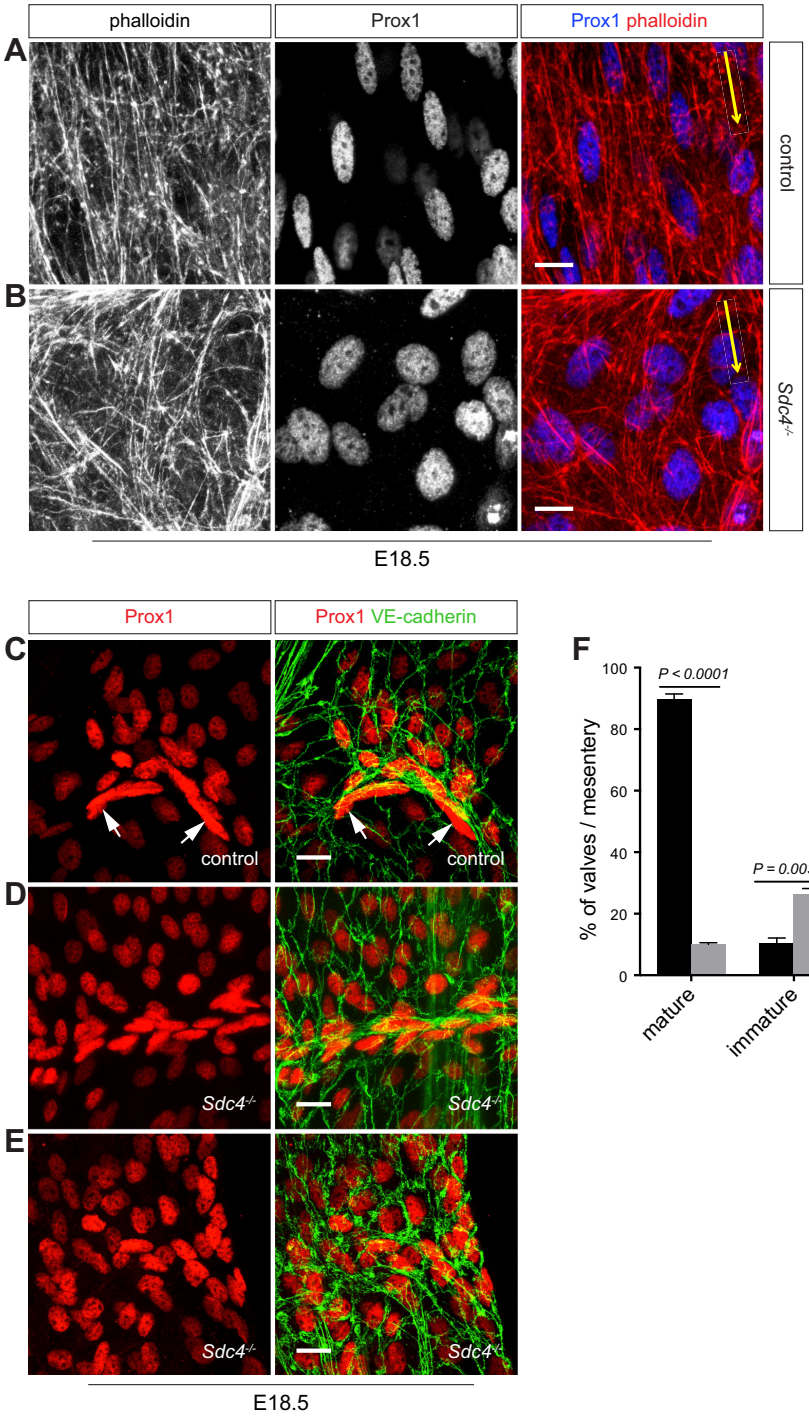

Fig. 2. Abnormal alignment of actin filaments and compromised formation of lymphatic valves in *Sdc4*$^{-/-}$ mice. (A) Phalloidin labeling showing that long, fine actin fibers of LECs align with the flow direction in control animals. (B) In *Sdc4* nulls, actin filaments are thick, short and randomly organized. Yellow arrows (A,B) indicate flow direction in lymphatic vessel. (C) Representative V-shaped mature lymphatic valves in control mice (arrows). (D,E) Ring-shaped immature lymphatic valves (D) and abnormal valves consisting of randomly oriented Prox1^{high} lymphatic valve-forming ECs (E) in *Sdc4*$^{-/-}$ animals. (F) Quantification of lymphatic valves formed in mesentery at E18.5 based on Prox1 and VE-cadherin staining. The proportion (%) of different types of valves relative to the total number of valves formed per mesentery is shown. V-shaped valves are defined as mature valves. Immature valves are ring-shaped. Valves consisting of randomly organized Prox1^{high} valve-forming ECs or Prox1^{high} cells remaining parallel to the flow direction are considered as abnormal valves. Student's *t*-test (two-tailed). Data are mean±s.e.m. (n=3). Scale bars: 10 µm in A,B; 15 µm in C-E.

(Fig. S8). However, the increase was much more extensive in *Sdc4*$^{-/-}$; *Pecam1*$^{-/-}$ double knockouts (Fig. 5B,C). Moreover, *Sdc4*$^{-/-}$; *Pecam1*$^{-/-}$ mice developed abnormal lymphatic valves (Fig. 5D-F).

To investigate whether there is any compensation between Sdc4 and Pecam1, we examined *Pecam1* levels in lymphatic vessels of *Sdc4*$^{-/-}$ mice or *Sdc4* levels in *Pecam1*$^{-/-}$ mice by qRT-PCR. No significant changes in expression were observed (Fig. S9A,B).

Vangl2 expression is upregulated in *Sdc4*$^{-/-}$ mice

The reorientation defect of Prox^{high} valve-forming ECs observed in *Sdc4*$^{-/-}$ or *Pecam1*$^{-/-}$ mutants is reminiscent of mice deficient in the PCP protein Vangl2 (Tatin et al., 2013). We therefore measured VANGL2 expression in *SDC4* knockdown (KD) or *PECAM1* KD LECs. Exposure to laminar flow increased VANGL2 levels in controls as well as in *SDC4* KD and *PECAM1* KD LECs (Fig. 6A). However, the increase was much higher in *SDC4* KD LECs compared with controls (7-fold versus 3-fold), while the increase was less marked in *PECAM1* KD cells (Fig. 6A).

Similar results were observed *in vivo*. We isolated thoracic duct (TD) from wild-type (WT) and *Sdc4*$^{-/-}$ mice and examined the expression levels of *Vangl2* by qRT-PCR. Since TD contains a mixed pool of cell types, we normalized our qRT-PCR results to *Cdh5* (Fig. 6B). There was a significant (5.8-fold) increase in *Vangl2* expression in *Sdc4*$^{-/-}$ compared with WT mice (Fig. 6B). In

Development (2016) 143, 4441-4451 doi:10.1242/dev.140129

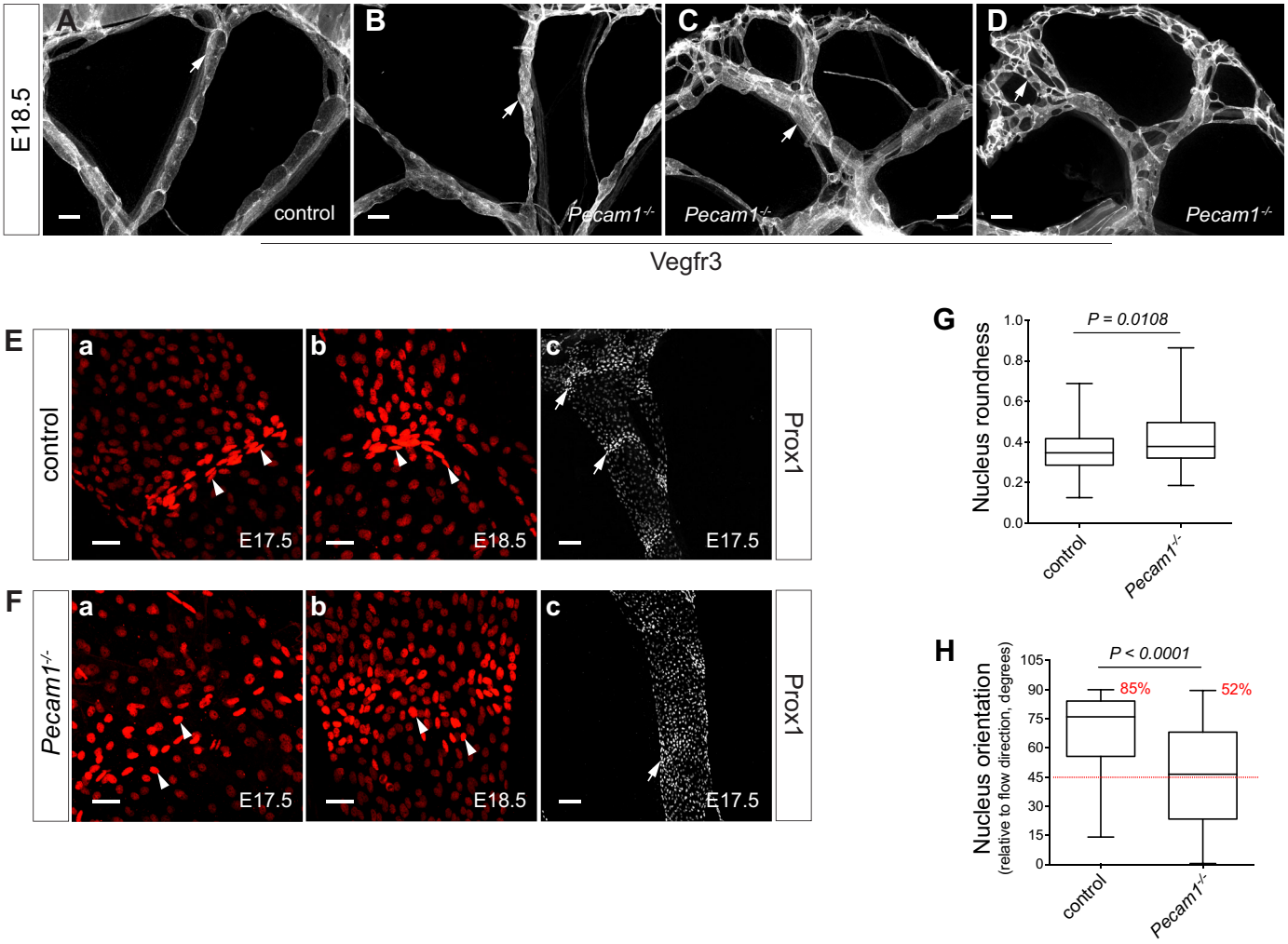

Fig. 3. *Pecam1*$^{-/-}$ mice show lymphatic remodeling defects at E18.5. (A-D) Irregular (B, arrow), enlarged (C, arrow) and abnormally branched (D, arrow) mesenteric lymphatic vessels developed in *Pecam1*$^{-/-}$ mice but not in controls (A, arrow) at E18.5. (E,F) Compared with control (Ea,b, arrowheads), the nuclei of Prox1^{high} valve-forming cells in *Pecam1*$^{-/-}$ are less elongated (Fa,b, arrowheads), randomly oriented and loosely organized. Nuclei of Prox1^{high} valve-forming cells aligned along the longitudinal axis of lymphatic vessels were also seen in *Pecam1*$^{-/-}$ embryos (Fc, arrow). In control mice, by contrast, the nuclei of Prox1^{high} valve-forming cells are concentrated in valve areas (Ec, arrows). (G) Quantification of nuclear shape (roundness) of Prox1^{high} cells in E17.5 mesenteric lymphatic vessels (n=5). Mann–Whitney test. (H) Nuclear orientation of Prox1^{high} cells in E17.5 mesenteric lymphatic vessels (n=5). The percentage of nuclei reoriented >45° relative to flow direction is indicated. Mann–Whitney test. Scale bars: 200 µm in A-D; 30 µm in Ea,b,Fa,b; 100 µm in Ec,Fc.

addition, there was a less profound (2.6-fold) increase in *Celsr1*, which encodes a PCP protein, in *Sdc4* nulls (Fig. 6B), whereas *Celsr1* levels in *Pecam1*$^{-/-}$ mice appeared similar to those in WT (Fig. S9C). To examine whether increased Vangl2 levels in *Sdc4* nulls mediate increased *Celsr1* expression, we overexpressed VANGL2 in LECs (Fig. S9D) and measured *CELSR1* expression in these cells using qRT-PCR. VANGL2 overexpression resulted in an increase in *CELSR1* levels (Fig. S9E) that was similar to that shown *in vivo* above.

SDC4 controls LEC response to flow signals through VANGL2

We postulated that an increase in Vangl2 levels was responsible for the mis-sensing of flow signals in *Sdc4* null LECs, leading to lymphatic vessel remodeling defects. To test this hypothesis, we first examined whether increased VANGL2 expression in LECs causes abnormal cell alignment to the direction of flow. LECs were transduced with a lentivirus expressing VANGL2 (pLenti-VANGL2) or control virus and cell alignment was evaluated after exposure to flow. Since the flow is largely laminar in lymphatic vessels before mature functional valves have developed, we subjected LECs to laminar flow *in vitro*. In the absence of flow (static condition), LECs are randomly oriented and thus display an average orientation of ∼45° relative to flow direction (perfect alignment of all cells with flow direction is 0°, and perpendicular alignment is 90°). LECs transduced with a control virus aligned normally to flow direction, with an average orientation of ∼33°, whereas VANGL2 overexpression almost fully inhibited the ability of the cells to align to flow, with an average orientation of ∼43°, close to the value measured in cells that were not exposed to flow (Fig. 6C-E).

To relate the abnormal polarization of lymphatic valve-forming ECs in *Sdc4*$^{-/-}$ mice to a flow sensing defect, we tested the ability of LECs with reduced Sdc4 expression to align under flow. Primary LECs were transfected with scrambled siRNA (siScrambled) or siRNA against *SDC4* (siSDC4) (Fig. S10A,B) and subjected to laminar flow (8 dynes/cm^2). After 16 h of flow exposure, control LECs (transfected with siScrambled) were elongated along the flow axis, with phalloidin labeling demonstrating remodeling of actin

Development (2016) 143, 4441-4451 doi:10.1242/dev.140129

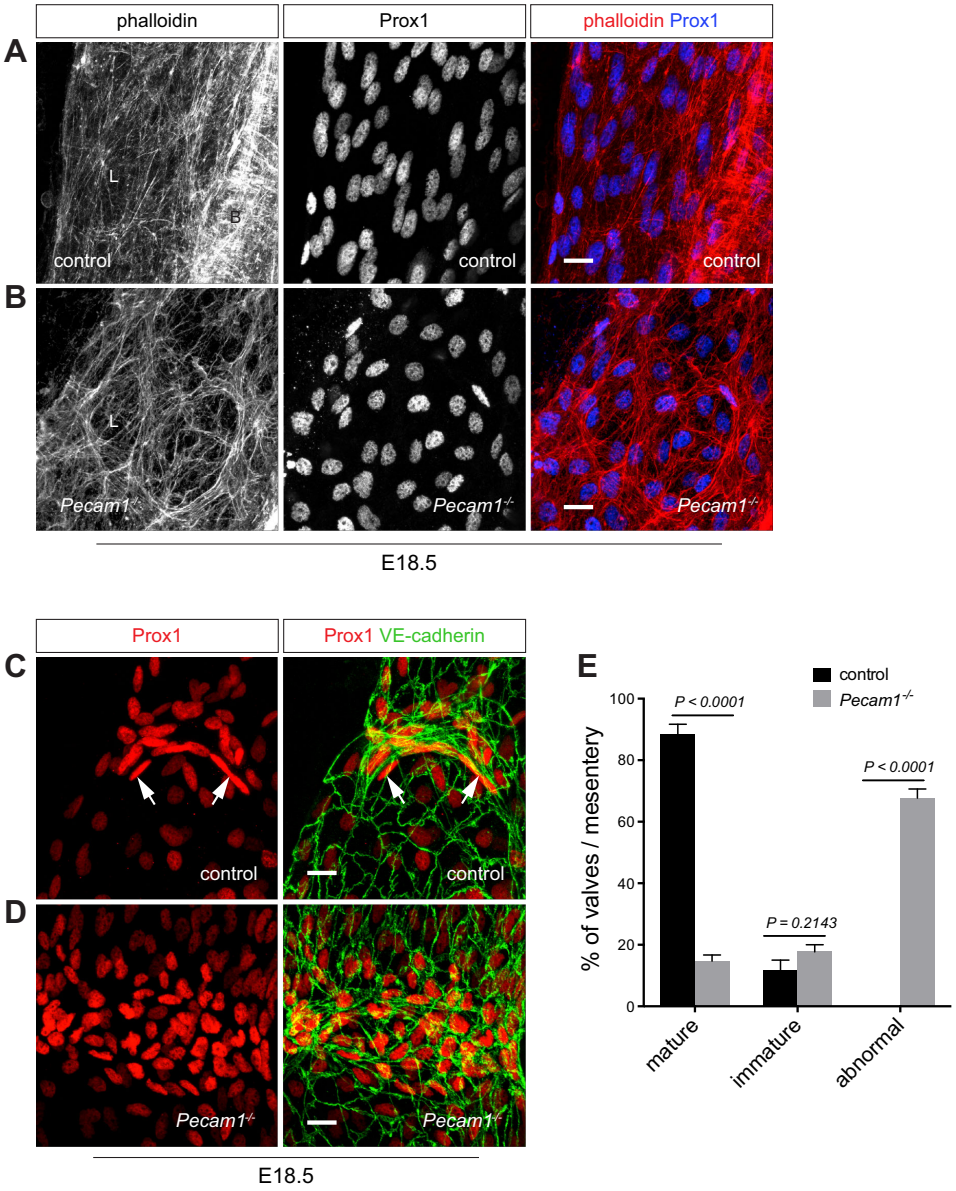

Fig. 4. Disorganized actin stress fibers and reduced formation of mature lymphatic valves in *Pecam1*$^{-/-}$ mice at E18.5. (A) Long, fine actin filaments labeled by phalloidin align to flow direction in lymphatic vessels (Prox1^{+}) in control mice. B, blood vessel; L, lymphatic vessel. (B) In *Pecam1*$^{-/-}$ embryos, actin fibers exhibit a short, thick appearance, and do not align. (C) Immunofluorescence staining showing V-shaped mature lymphatic valves (arrows) in the mesentery in control mice. (D) Abnormal lymphatic valves containing randomly oriented Prox1^{high} valve-forming ECs were observed in *Pecam1* knockouts. (E) Quantification of lymphatic valves formed in E18.5 mesentery based on staining for Prox1 and VE-cadherin. The proportion (%) of different types of valves relative to the total number of valves formed per mesentery is shown. Mature valves are V-shaped; immature valves are ring shaped; abnormal valves are those consisting of randomly organized Prox1^{high} valve-forming cells or Prox1^{high} valve-forming cells aligned parallel to the longitudinal axis of lymphatic vessels. Student's *t*-test (two-tailed). Data represent mean±s.e.m. (*n*=3). Scale bars: 15 µm.

fibers into long, fine filaments (Fig. 7A,B). By contrast, LECs transfected with siSDC4 (*SDC4* KD LECs) exhibited a cuboidal morphology, with the actin fibers in these cells retaining a thick and short appearance, and failed to align along the direction of flow (Fig. 7B).

Measurements of cell orientation in response to laminar flow confirmed these observations. When subjected to flow, control LECs aligned to flow with the average orientation between 35° and 40° relative to flow direction (Fig. 7C, siScrambled). By contrast, flow had no effect on the alignment of *SDC4* KD LECs, which showed an average orientation of ∼45°, similar to cells that were not subjected to flow (static) (Fig. 7C, siSDC4). Remarkably, reducing VANGL2 levels in *SDC4* KD LECs restored their ability to align under flow (Fig. 7B,C, siSDC4; siVANGL2). In fact, these cells aligned as well as control cells (Fig. 7B,C).

We also examined flow-mediated activation of VEGFR3 signaling in control and *SDC4* KD LECs (Fig. S10C). As expected, flow activated VEGFR3 signaling in control LECs (Fig. S10C). By contrast, flow-induced activation of VEGFR3 signaling was significantly reduced in *SDC4* KD cells (Fig. S10C).

DISCUSSION

The data presented in this study identify two new regulators of FSS-mediated lymphatic vasculature remodeling: Sdc4 and Pecam1. A deletion of either gene in mice resulted in a similar lymphatic remodeling defect during embryonic development. Moreover, simultaneous deletion of both genes caused a more severe lymphatic phenotype that included the appearance of blood-filled jugular lymph sac at E15.5. This phenotype is unlikely to be secondary to blood vessel defects, as hemorrhage or other obvious blood vessel abnormalities were not seen in these animals. One potential explanation is the formation of abnormal lympho-venous valves, resulting in blood backflow into the lymphatic vascular network. Another phenotype observed in *Sdc4*$^{-/-}$ or *Pecam1*$^{-/-}$ embryos was an increase in mural cell coverage in lymphatic vessels and this was even more pronounced in *Sdc4*$^{-/-}$; *Pecam1*$^{-/-}$ double nulls. These data support the existence of abnormal flow signaling in these mutants and are consistent with a previous report (Sweet et al., 2015). The enlarged lymphatic vessel diameter in *Sdc4*$^{-/-}$ embryos has been linked with increased LEC proliferation. This is not the case in *Pecam1* nulls. Although *Sdc4*$^{-/-}$ and some *Sdc4*$^{-/-}$;

Development (2016) 143, 4441-4451 doi:10.1242/dev.140129

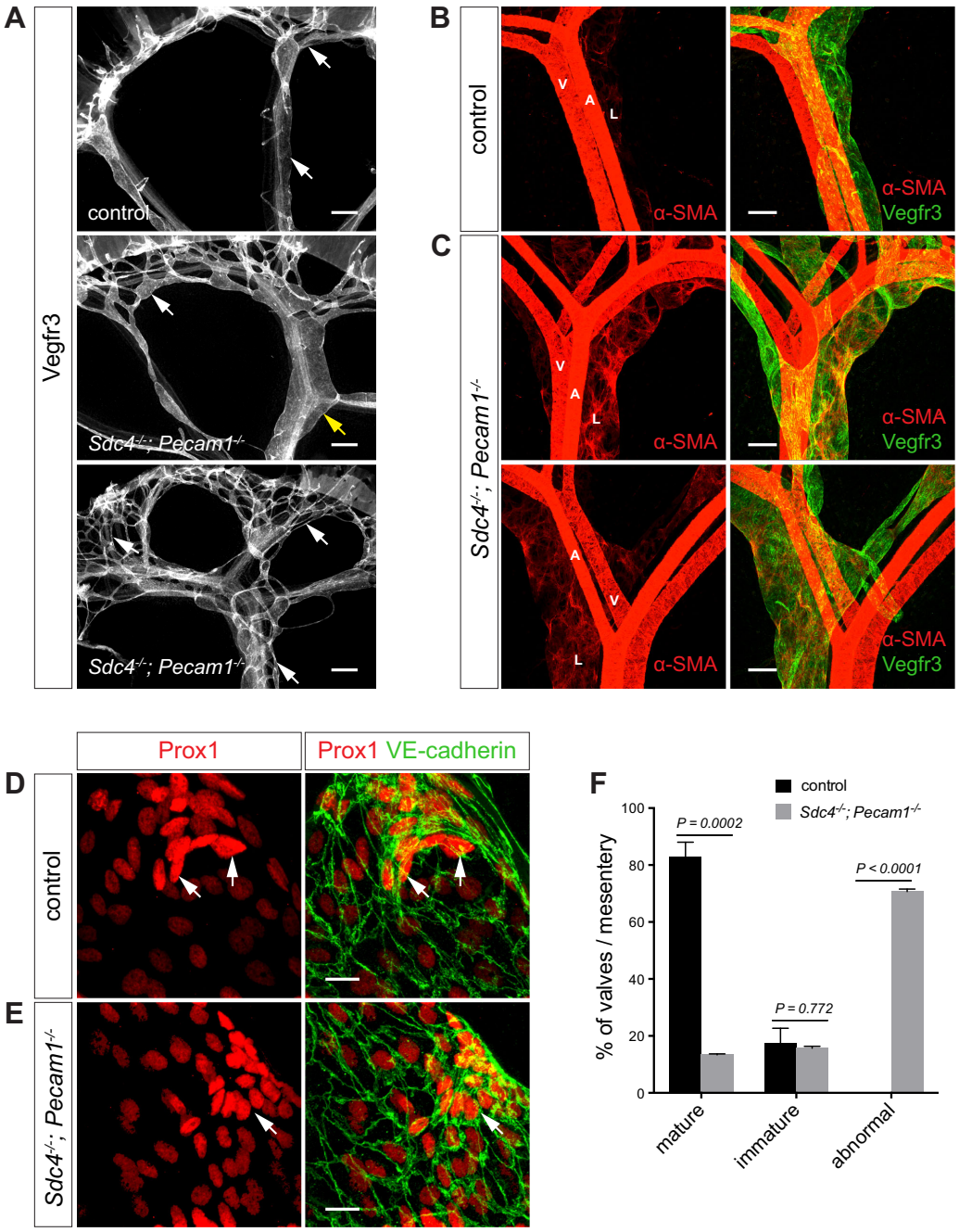

Fig. 5. *Sdc4*$^{-/-}$; *Pecam1*$^{-/-}$ double nulls show a severe lymphatic phenotype. (A) Mesenteric lymphatic vessels in *Sdc4*$^{-/-}$; *Pecam1*$^{-/-}$ embryos show irregular morphology (middle, white arrow), increased diameter (middle, yellow arrow) and abnormal branching (bottom, arrows) at E18.5, which were not seen in controls (top, arrows). (B) Sparse mural cell (α-SMA^{+}) coverage in mesenteric lymphatic vessels in control mice at E18.5. (C) Extensive mural cell recruitment in lymphatic vessels of *Sdc4*$^{-/-}$; *Pecam1*$^{-/-}$ double nulls. A, artery; V, vein; L, lymphatic vessel. (D) Mature V-shaped valves in mesenteric lymphatic vessels of control mice at E18.5 (arrows). (E) Abnormal lymphatic valves containing randomly oriented Prox1^{high} valve-forming ECs formed in *Sdc4*$^{-/-}$; *Pecam1*$^{-/-}$ mice at E18.5 (arrows). (F) Quantification of lymphatic valves formed in the mesentery of control and *Sdc4*$^{-/-}$; *Pecam1*$^{-/-}$ mice at E18.5 according to antibody staining for Prox1 and VE-cadherin. The proportion (%) of different types of valves relative to the total number of valves formed per mesentery is shown. Mature valves are V-shaped; immature valves are ring shaped; abnormal valves are those consisting of randomly organized Prox1^{high} valve-forming cells or Prox1^{high} cells aligned parallel to the longitudinal axis of lymphatic vessels. Student's *t*-test (two-tailed). Data represent mean±s.e.m. (*n*=3). Scale bars: 200 µm in A; 100 µm in B,C; 15 µm in D,E.

Pecam1$^{-/-}$ double-knockout mice can survive to adulthood, the presence of abnormal lymphatic valves in the adult may affect the function of lymphatic vessels leading to increased morbidity (Alexander et al., 2010).

The more severe lymphatic phenotype that developed in *Sdc4*$^{-/-}$; *Pecam1*$^{-/-}$ double nulls suggests that Sdc4 and Pecam1 function through independent flow signaling pathways. While both have been implicated in flow signaling in LECs, the molecular mechanisms involved are distinct: in the case of Sdc4, it involves regulation of flow-mediated Vangl2 expression, whereas PCP proteins do not seem to be involved in Pecam1-controlled flow signaling (Fig. S11).

Development (2016) 143, 4441-4451 doi:10.1242/dev.140129

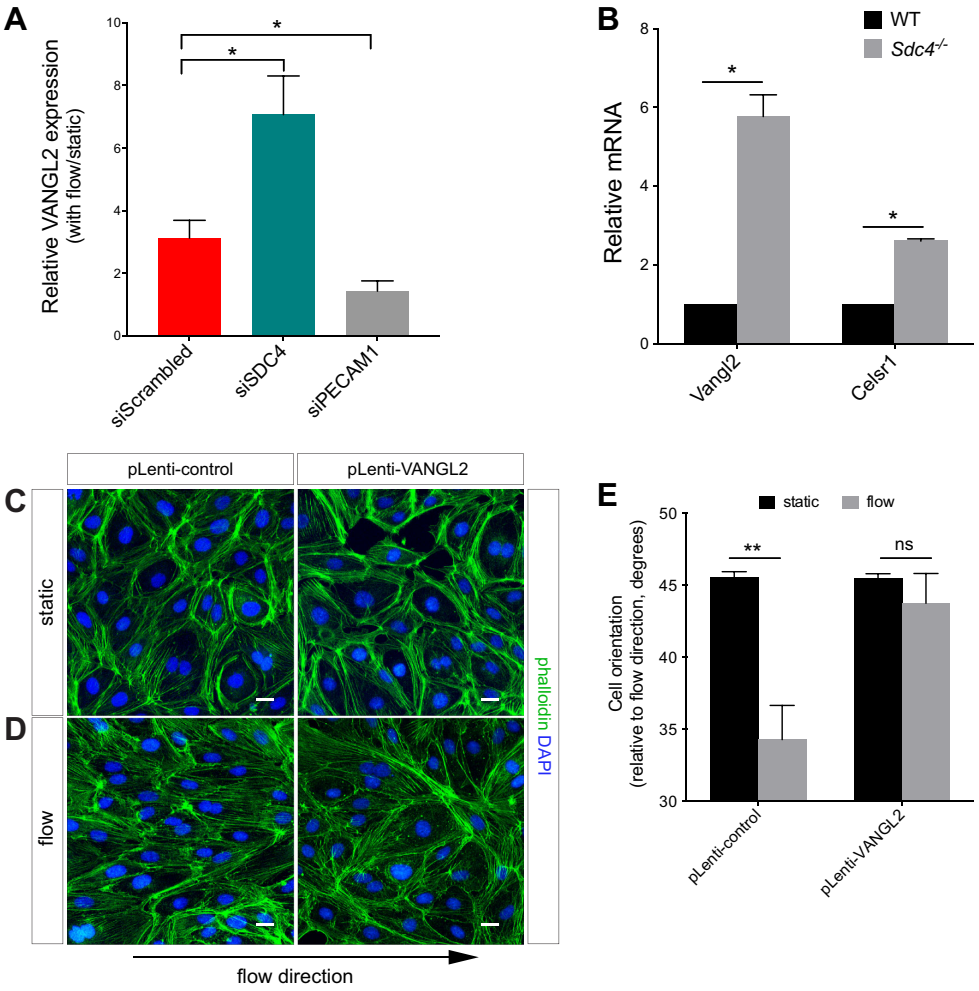

Fig. 6. The PCP protein Vangl2 is upregulated in LECs in *Sdc4*$^{-/-}$ mice. (A) qRT-PCR analysis of relative *VANGL2* expression in human LECs after being subjected to laminar flow (8 dynes/cm^2) for 20 h versus static cells. mRNA expression was normalized to endogenous β-actin (*ACTB*). Mann–Whitney test (*n*=6). **P*<0.05. Values represent mean±s.e.m. (B) qRT-PCR for *Vangl2* and *Celsr1* in thoracic ducts of WT and *Sdc4*$^{-/-}$ mice. mRNA expression was normalized to endogenous 18S rRNA and *Cdh5*. Mann–Whitney test (*n*=4). **P*<0.05. Values are mean±s.e.m. (C,D) Visualization of the orientation of control LECs (pLenti-control) (left) and cells overexpressing VANGL2 (pLenti-VANGL2) (right) by phalloidin labeling (green) and DAPI staining (blue). VANGL2-overexpressing LECs do not align to flow direction (D, right). Scale bars: 20 µm. (E) Quantification of cell orientation of control and VANGL2-overexpressing LECs. Cells were either maintained in no flow conditions (static) or subjected to laminar flow (8 dynes/cm^2) for 16 h. One-way ANOVA. ns, not significant; ***P*<0.01. *n*>2700 cells/condition/experiment. Four independent experiments were performed. Values are mean±s.e.m.

PECAM1 involvement in mechanotransduction is well established in BECs, where it transduces shear forces to activate a complex with VE-cadherin and VEGF receptor to mediate shear stress signaling (Tzima et al., 2005). However, its involvement in flow sensing events in the lymphatic endothelium has not been reported previously. A recent study has demonstrated that the transmembrane domain of VE-cadherin can bind directly to the transmembrane domains of VEGFR2 and VEGFR3 (Coon et al., 2015), suggesting that VEGFR3, which is highly expressed in LECs, could be a component of a mechanotransduction complex. This is supported by the observation that changes in Vegfr3 levels in mice and zebrafish modulate aortic lumen diameter in a flow-dependent manner (Baeyens et al., 2015). The lymphatic remodeling defects observed in this study in *Pecam1* knockout mice point to the importance of FSS-mediated signals in lymphatic vasculature development. The similarity in the lymphatic abnormalities that developed in *Sdc4*$^{-/-}$ and *Pecam1*$^{-/-}$ mice suggests that the lymphatic vascular defects in *Sdc4* nulls are also due to impaired flow sensing in LECs.

The role of Pecam1 in flow sensing has been extensively investigated, whereas relatively little is known about Sdc4 involvement in this process. We recently demonstrated that aortic ECs of *Sdc4* null mice are poorly aligned in the direction of flow and that *SDC4* KD in human umbilical vein ECs inhibits flow-induced alignment, a defect rescued by re-expression of the gene (Baeyens et al., 2014).

Surprisingly, the PCP protein Vangl2 was identified as an important component of Sdc4-dependent shear stress signals in this study. Laminar flow upregulates VANGL2 expression in LECs *in vitro*, indicating that VANGL2 is a flow-responsive gene. Consistent with this observation, flow had only minimal effects on VANGL2 expression in *PECAM1* KD LECs, which are defective in transducing mechanical forces. However, in the setting of reduced SDC4 expression, exposure to flow led to a much greater increase in VANGL2 expression than that seen in control LECs. Increased Vangl2 levels were also observed in lymphatic vessels in *Sdc4* null mice. These results suggest that SDC4 controls the extent of flow-induced increase in VANGL2 expression.

The excessive increase in VANGL2 expression in response to flow in LECs with reduced SDC4 expression accounts for the misalignment of these cells. Indeed, VANGL2 overexpression in control (WT) LECs impaired their ability to align to flow, while the reduction of VANGL2 expression in *SDC4* KD LECs restored their ability to align. Combined with observations of abnormal lymphatic valve morphogenesis in *Vangl2*-deficient mice (Tatin et al., 2013), these data suggest that there is an optimal level of Vangl2 expression in LECs. The concept of the optimal expression level of a particular protein with regard to the regulation of flow-mediated cell alignment is consistent with a recent description of an endothelial flow-sensing set-point study (Baeyens et al., 2015).

The involvement of PCP proteins in lymphatic valve morphogenesis has been reported previously. Ablation of the

Development (2016) 143, 4441-4451 doi:10.1242/dev.140129

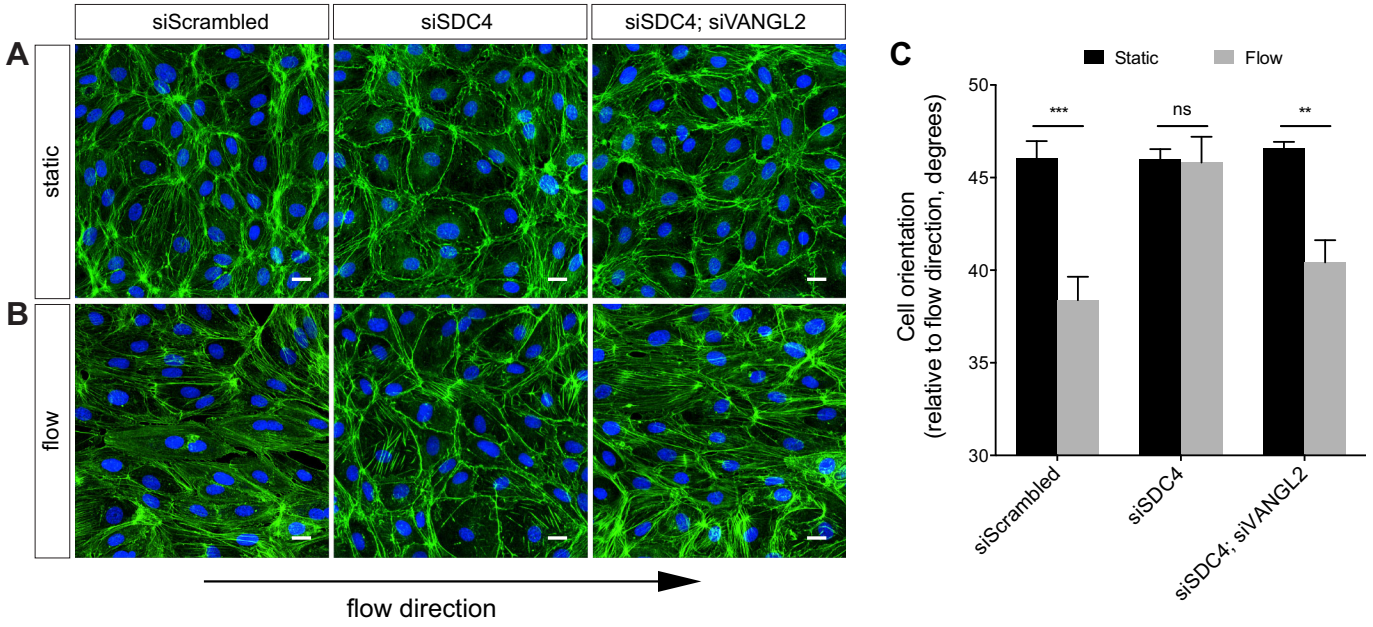

Fig. 7. SDC4 controls flow sensing in LECs through VANGL2. (A,B) Phalloidin labeling (green) and DAPI staining (blue) show the arrangement of human LECs under static conditions (A) and sheared with laminar flow (8 dynes/cm^2) for 16 h (B). Scale bars: 20 µm. (C) Quantification of cell orientation of LECs transfected with a scrambled, *SDC4*, or *SDC4* and *VANGL2* siRNA. Cells were either cultured at a no flow condition (static) or subjected to laminar flow (8 dynes/cm^2) for 16 h. Two-way ANOVA. ns, not significant; ***P*<0.01, ****P*<0.001. *n*>1800 cells/condition/experiment. Four independent experiments were performed. Values are mean±s.e.m.

core PCP proteins Celsr1 or Vangl2 in mice results in the formation of abnormal lymphatic valves due to a reorientation defect of lymphatic valve-forming cells (Tatin et al., 2013). Moreover, Vangl2 has been shown to be involved in flow-controlled ependymal cilia orientation (Guirao et al., 2010), suggesting that this PCP protein plays a role in the integration of FSS-mediated signals. Yet, how it achieves this effect remains unknown. Our results expand this concept by demonstrating that *VANGL2* is a flow-responsive gene and its expression levels, as induced by flow, are critical for LECs to align to flow. We have further identified that SDC4 is an important regulator in this process.

The need for an optimal Vangl2 level controlling cell orientation is consistent with what is known about PCP protein involvement in cell polarization. In vertebrate inner ear hair cells, the core PCP proteins Frizzled (Fz) and Dishevelled (Dvl) form a complex on one side of the cell that is opposite to Van Gogh (Vangl) and Prickle (Pk) on the other. This asymmetric distribution of the PCP proteins is required for hair cell polarization (Deans et al., 2007; Etheridge et al., 2008; Montcouquiol et al., 2006; Wang et al., 2006; Yin et al., 2012). Increased Vangl2 levels in *Sdc4*$^{-/-}$ LECs may disrupt PCP protein distribution in the cells, resulting in abnormal cellular orientation.

The appearance of 'wavy' endothelial cell-cell junctions in the lymphatic vessels of *Sdc4*$^{-/-}$ mice is consistent with a degree of destabilization. Indeed, the involvement of PCP proteins in controlling classical cadherins has been reported previously (Nagaoka et al., 2014a,b). In the nervous system, Vangl2 binds directly to the intracellular domain of N-cadherin to stabilize cell-cell junctions (Nagaoka et al., 2014b). Similarly, Vangl2 controls E-cadherin in epithelial cells (Nagaoka et al., 2014a). It is therefore likely that, in LECs, Vangl2 binds VE-cadherin to regulate the formation of endothelial adherens junctions.

In summary, our study has identified a new mechanism of FSS-mediated signaling that involves Sdc4-dependent upregulation of the PCP protein Vangl2 driven by flow.

MATERIALS AND METHODS

Mice

Sdc4$^{-/-}$ and *Pecam1*$^{-/-}$ strains were maintained in a C57BL/6J background. *Sdc4*$^{-/-}$; *Pecam1*$^{-/-}$ mice were generated by breeding *Sdc4*$^{+/-}$; *Pecam1*$^{-/-}$ with *Sdc4*$^{+/-}$; *Pecam1*$^{-/-}$. The morning that the vaginal plug was found is designated embryonic day (E) 0.5. All mouse experiments complied with protocols approved by the Yale University Institutional Animal Care and Use Committee.

Whole-mount immunofluorescence staining and image acquisition

For whole-mount immunofluorescence staining of mesentery, tissue was fixed in 1% paraformaldehyde (PFA) for 1 h at room temperature, then washed with ice-cold PBS three times. Tissue was blocked in blocking buffer comprising 5% donkey serum, 0.2% BSA, 0.3% Triton X-100 in PBS for 1 h at room temperature, then incubated with primary antibody diluted in blocking buffer overnight at room temperature. After washing with wash buffer comprising 0.3% Triton X-100 in PBS, tissue was incubated with secondary antibody diluted in blocking buffer at 4°C overnight. Tissue was then washed with wash buffer and flat mounted using fluorescent mounting medium (DAKO). Images were acquired using a Leica DM6000 CS confocal or Nikon Eclipse 80i microscope. Confocal images are maximum intensity projections of *z*-stacks. Nuclear orientation and shape (roundness) of Prox1^{high} valve-forming ECs were quantified using ImageJ (NIH).

Primary antibodies were: rabbit anti-Prox1 (11,002, AngioBio, 1:200), rabbit anti-Lyve1 (11-034, AngioBio, 1:400), rabbit anti-laminin α5 (Ringelmann et al., 1999) (1:1000), rat anti-VE-cadherin (clone 11D4.1, 555289, BD Biosciences, 1:100), goat anti-Vegfr3 (AF743, R&D Systems, 1:100), hamster anti-podoplanin (Developmental Studies Hybridoma Bank, University of Iowa, 1:1000) and Cy3-conjugated αSMA (clone 1A4, C6198, Sigma-Aldrich, 1:400); Alexa Fluor 488-conjugated phalloidin was used to stain actin (A12379, Life Technologies, 1:200).

Development (2016) 143, 4441-4451 doi:10.1242/dev.140129

Secondary antibodies were: Alexa 647-conjugated chicken anti-rabbit (A-21443, Invitrogen, 1:200), Alexa 594-conjugated chicken anti-rabbit (A-21442, Invitrogen, 1:200), Alexa 488-conjugated chicken anti-goat (A21467, Invitrogen, 1:200), Alexa 488-conjugated donkey anti-rat (A-21208, Invitrogen, 1:200) and Alexa 647-conjugated goat anti-hamster (A21451, Invitrogen, 1:200).

Cell culture and siRNA transfection

Human dermal LECs (Lonza, CC-2812) were used in this study, and were cultured in EGM-2MV medium (Lonza, CC-3202). For gene KD in LECs, cells were transfected with siRNAs using Lipofectamine RNAiMAX (Invitrogen) according to the manufacturer's instructions. siRNA was washed out 6-8 h after transfection. Transfected cells were harvested for experiments 72 h after transfection.

siRNAs used for gene KD were from OriGene Technologies: scrambled siRNA (NC1 Control SR30004) and siRNA against human *SDC4* (SR304301), human *VANGL2* (SR311428) or human *PECAM1* (SR303439), each at 15 nM.

Lentiviral transduction

LECs were transduced with lentiviral particles expressing control (OHS5833, GE Healthcare Dharmacon) or VANGL2 (OHS5899-202624111, GE Healthcare Dharmacon). Protein expression was identified by immunoblot analysis.

qRT-PCR analysis

cDNA was synthesized from 1 µg total RNA using the Superscript III First-Strand Synthesis System (Invitrogen) following the manufacturer's instructions. 3 µl cDNA was used for each qPCR reaction, which was performed in a 25 µl reaction volume in triplicate on a CFX96 Real-Time System C1000 thermal cycler (Bio-Rad) using iQ SYBR Green Supermix (Bio-Rad). Four independent experiments were carried out. The cycle employed an initial denaturation step at 95°C for 10 min, followed by 40 cycles at 95°C for 15 s and 60°C for 1 min. qPCR primers for human *VANGL2* were purchased from Qiagen (PPH12377B-200). Other primers were as follows (5′-3′, forward and reverse): mouse *Vangl2*, CCAGCCG-CTTCTACAATGTC and TCTCCAGGATCCACACTGC; mouse *Celsr1*, GGCAGTCATGACCTTGGACTA and AGCTGATTCCCAATCTGCAC; mouse *Sdc4*, CATCTTTGAGAGAACTGAGGTCTTG and CCTTCTTC-TTCATGCGGTACA; mouse *Pecam1*, CGGTGTTCAGCGAGATCC and ACTCGACAGGATGGAAATCAC; mouse 18S rRNA (*Rn18s*), AGGAA-TTCCCAGTAAGTGCG and GCCTCACTAAACCATCCAA; human *ACTB*, CCAACCGCGAGAAGATGA and CCAGAGGCGTACAGGGATAG; human *SDC4*, GGCAGGAATCTGATGACTTTG and GCCGATCAT-GGAGTCTTCC; human *CELSR1*, TGGATATCTCCAGGCGTGA and AGCGGCATAGGTGACAATCT.

Isolation of total RNA from thoracic duct

Thoracic ducts were dissected out from ten adult WT and ten adult *Sdc4*$^{-/-}$ mice and were collected in RLT Plus Buffer (Qiagen). Tissue was homogenized using TissueLyser II (Qiagen) followed by centrifugation at 15,000 rpm (21,000 ***g***) at 4°C. Supernatant was collected, from which total RNA was extracted using the RNeasy Plus Mini Kit (Qiagen).

Fluorescence-activated cell sorting

Mesenteric vessels of E18.5 control, *Sdc4*$^{-/-}$ or *Pecam1*$^{-/-}$ embryos were digested for 30 min at 37°C in 1 mg/ml collagenase type II with periodic gentle inversion to mix, followed by mechanical dissociation via repeated pipetting. Single cells were incubated in 10 µg/ml Hoechst 3342 (Sigma) for 30 min at 37°C, followed by an additional 15 min incubation with 0.5 µg/ml Pyronin Y (Sigma) and fluorescently conjugated antibodies Pecam1 (CD31)-FITC, VE-cadherin (CD144)-FITC, CD45-PECy7 and Lyve1-Alexa 647. ECs were identified as events negative for CD45 (Ptprc) and positive for either the Pecam1 (*Sdc4*$^{-/-}$ experiments) or VE-cadherin (*Pecam1*$^{-/-}$ experiments) endothelial marker; LECs were subsequently discriminated as Lyve1^{+}. Two-dimensional cell cycle FACS analysis was then performed on BEC and LEC events by comparing DNA (Hoechst) and RNA (Pyronin Y) content.

Western blotting analysis

Cells were rapidly washed with ice-cold PBS twice and lysed with 100 µl RIPA lysis buffer containing complete mini EDTA-free protease inhibitors (11836170001, Roche) and phosphatase inhibitors (04906837001, Roche). Cell lysates were subjected to two cycles of snap-freezing in liquid nitrogen and then cleared by centrifugation at 15,000 rpm (21,000 ***g***) for 10 min. Protein concentration was determined using BCA protein assay (Thermo Scientific) and equalized in each sample. Then, 40 µg total protein from each sample was loaded onto a 4-15% TGX gel (Bio-Rad) with Tris/glycine/SDS buffer (Bio-Rad) for SDS-PAGE and transferred to an Immobilon-P (PVDF) membrane (IPVH 00010, Millipore). Membranes were blocked with 5% non-fat dried milk (AB 10109-01000, AmericanBio) in Tris-buffered saline containing 0.05% Tween 20 (TBS-T) for 1 h at room temperature and then incubated with primary antibodies at 4°C overnight. Membranes were washed with TBS-T and incubated with secondary antibodies for 2 h at room temperature. Protein bands were visualized using HRP-conjugated secondary antibodies by enhanced chemiluminescence (Immobilon Western Chemiluminescent HRP Substrate, WBKL S0500, Millipore) recorded using a digital acquisition system (G-Box, Syngene) equipped with a CCD camera with 'true' 1.4 megapixel resolution.

Primary antibodies were: anti-syndecan 4 (Abcam, ab24511, 1:1000), anti-actin (Santa Cruz, sc-1615, 1:200), anti-VANGL2 (R&D Systems, AF4815, 1:100), anti-VEGFR3 (Cell Signaling Technology, 2638, 1:1000), anti-phospho-VEGFR3 (Cell Applications, cy1115, 1:1000) and anti-β-actin (Sigma, A1978, 1:10,000). Peroxidase-labeled secondary antibodies (all 1:2000) were: goat anti-rabbit IgG (Vector Laboratories, PI-1000), horse anti-goat IgG (Vector Laboratories, PI-9500), rabbit anti-sheep IgG (Thermo Scientific, 31480) and horse anti-mouse IgG (Vector Laboratories, PI-2000).

Shear stress

LECs were seeded on fibronectin-coated (20 µg/ml) tissue culture plastic slides. On reaching confluence, cells were starved with EBM-2 medium (Lonza, CC-3156) containing 5% FBS, 100 U/ml penicillin and 100 µg/ml streptomycin for 4 h. Shear stress with a calculated intensity of 8 dynes/cm^2 was applied in a parallel flow chamber with starvation medium. After 16 or 20 h of steady laminar flow, cell alignment was quantified by measuring nuclear orientation using a custom-made MATLAB (MathWorks) function (Baeyens et al., 2014). At least 50 images/condition/experiment taken with a 20× objective were used for quantification.

Statistical analysis

GraphPad Prism 6 was used for statistical analysis. Student's *t*-test (two-tailed), Mann–Whitney test, Kruskal–Wallis test, one-way ANOVA and two-way ANOVA were applied to determine statistical significance.

Acknowledgements

We thank Eleni Tzima for *Pecam1*$^{-/-}$ mice, Anne Eichmann for helpful discussion, Lydia Sorokin for laminin α5 antibody and Gyong Ju Min for help with flow experiments.

Competing interests

The authors declare no competing or financial interests.

Author contributions

Y.W. carried out most of the experiments and prepared figures. N.B. conducted flow experiments and quantified the shape and the orientation of lymphatic valve-forming cells. F.C. performed western blotting. K.T. conducted flow experiments and western blotting. J.S.F. performed FACS. J.Z. isolated thoracic ducts from mice. Y.J. helped with analysis of lymphatic phenotypes. B.C. helped with flow experiments. K.K.H. and M.A.S. helped with data analysis, study design and manuscript preparation. Y.W. and M.S. designed the project and wrote the manuscript. M.S. supervised all aspects of the project.

Funding

This work was supported by the National Institutes of Health [R01 HL062289 to M.S., R01 HL075092 to M.A.S., R01 HL128064 to K.K.H.]; an American Heart Association Postdoctoral Fellowship [14POST19020010 to N.B.]; and Borsa di Studio Società Italiana di Farmacologia (SIF)-MSD Italia [to F.C.]. Deposited in PMC for release after 12 months.

Development (2016) 143, 4441-4451 doi:10.1242/dev.140129

Supplementary information

Supplementary information available online at
http://dev.biologists.org/lookup/doi/10.1242/dev.140129.supplemental

References

Alexander, J. S., Ganta, V. C., Jordan, P. A. and Witte, M. H. (2010). Gastrointestinal lymphatics in health and disease. *Pathophysiology* **17**, 315-335.

Astudillo, P., Carrasco, H. and Larraín, J. (2014). Syndecan-4 inhibits Wnt/β-catenin signaling through regulation of low-density-lipoprotein receptor-related protein (LRP6) and R-spondin 3. *Int. J. Biochem. Cell Biol.* **46**, 103-112.

Baeyens, N., Mulligan-Kehoe, M. J., Corti, F., Simon, D. D., Ross, T. D., Rhodes, J. M., Wang, T. Z., Mejean, C. O., Simons, M., Humphrey, J. et al. (2014). Syndecan 4 is required for endothelial alignment in flow and atheroprotective signaling. *Proc. Natl. Acad. Sci. USA* **111**, 17308-17313.

Baeyens, N., Nicoli, S., Coon, B. G., Ross, T. D., Van den Dries, K., Han, J., Lauridsen, H. M., Mejean, C. O., Eichmann, A., Thomas, J.-L. et al. (2015). Vascular remodeling is governed by a VEGFR3-dependent fluid shear stress set point. *Elife* **4**, e04645.

Bellin, R. M., Kubicek, J. D., Frigault, M. J., Kamien, A. J., Steward, R. L., Barnes, H. M., DiGiacomo, M. B., Duncan, L. J., Edgerly, C. K., Morse, E. M. et al. (2009). Defining the role of syndecan-4 in mechanotransduction using surface-modification approaches. *Proc. Natl. Acad. Sci. USA* **106**, 22102-22107.

Chen, C.-Y., Bertozzi, C., Zou, Z., Yuan, L., Lee, J. S., Lu, M. M., Stachelek, S. J., Srinivasan, S., Guo, L., Vincente, A. et al. (2012). Blood flow reprograms lymphatic vessels to blood vessels. *J. Clin. Invest.* **122**, 2006-2017.

Coon, B. G., Baeyens, N., Han, J., Budatha, M., Ross, T. D., Fang, J. S., Yun, S., Thomas, J.-L. and Schwartz, M. A. (2015). Intramembrane binding of VE-cadherin to VEGFR2 and VEGFR3 assembles the endothelial mechanosensory complex. *J. Cell Biol.* **208**, 975-986.

Deans, M. R., Antic, D., Suyama, K., Scott, M. P., Axelrod, J. D. and Goodrich, L. V. (2007). Asymmetric distribution of prickle-like 2 reveals an early underlying polarization of vestibular sensory epithelia in the inner ear. *J. Neurosci.* **27**, 3139-3147.

Elfenbein, A. and Simons, M. (2013). Syndecan-4 signaling at a glance. *J. Cell Sci.* **126**, 3799-3804.

Elfenbein, A., Lanahan, A., Zhou, T. X., Yamasaki, A., Tkachenko, E., Matsuda, M. and Simons, M. (2012). Syndecan 4 regulates FGFR1 signaling in endothelial cells by directing macropinocytosis. *Sci. Signal.* **5**, ra36.

Escobedo, N., Contreras, O., Muñoz, R., Farías, M., Carrasco, H., Hill, C., Tran, U., Pryor, S. E., Wessely, O., Copp, A. J. et al. (2013). Syndecan 4 interacts genetically with Vangl2 to regulate neural tube closure and planar cell polarity. *Development* **140**, 3008-3017.

Etheridge, S. L., Ray, S., Li, S., Hamblet, N. S., Lijam, N., Tsang, M., Greer, J., Kardos, N., Wang, J., Sussman, D. J. et al. (2008). Murine dishevelled 3 functions in redundant pathways with dishevelled 1 and 2 in normal cardiac outflow tract, cochlea, and neural tube development. *PLoS Genet.* **4**, e1000259.

Finsen, A. V., Lunde, I. G., Sjaastad, I., Østli, E. K., Lyngra, M., Jarstadmarken, H. O., Hasic, A., Nygård, S., Wilcox-Adelman, S. A., Goetinck, P. F. et al. (2011). Syndecan-4 is essential for development of concentric myocardial hypertrophy via stretch-induced activation of the calcineurin-NFAT pathway. *PLoS ONE* **6**, e28302.

Guirao, B., Meunier, A., Mortaud, S., Aguilar, A., Corsi, J.-M., Strehl, L., Hirota, Y., Desoeuvre, A., Boutin, C., Han, Y.-G. et al. (2010). Coupling between hydrodynamic forces and planar cell polarity orients mammalian motile cilia. *Nat. Cell Biol.* **12**, 341-350.

Horowitz, A., Tkachenko, E. and Simons, M. (2002). Fibroblast growth factor-specific modulation of cellular response by syndecan-4. *J. Cell Biol.* **157**, 715-725.

Montcouquiol, M., Sans, N., Huss, D., Kach, J., Dickman, J. D., Forge, A., Rachel, R. A., Copeland, N. G., Jenkins, N. A., Bogani, D. et al. (2006). Asymmetric localization of Vangl2 and Fz3 indicate novel mechanisms for planar cell polarity in mammals. *J. Neurosci.* **26**, 5265-5275.

Muñoz, R., Moreno, M., Oliva, C., Orbenes, C. and Larraín, J. (2006). Syndecan-4 regulates non-canonical Wnt signalling and is essential for convergent and extension movements in Xenopus embryos. *Nat. Cell Biol.* **8**, 492-500.

Nagaoka, T., Inutsuka, A., Begum, K., Bin hafiz, K. and Kishi, M. (2014a). Vangl2 regulates E-cadherin in epithelial cells. *Sci. Rep.* **4**, 6940.

Nagaoka, T., Ohashi, R., Inutsuka, A., Sakai, S., Fujisawa, N., Yokoyama, M., Huang, Y. H., Igarashi, M. and Kishi, M. (2014b). The Wnt/planar cell polarity pathway component Vangl2 induces synapse formation through direct control of N-cadherin. *Cell Rep.* **6**, 916-927.

Ohkawara, B., Glinka, A. and Niehrs, C. (2011). Rspo3 binds syndecan 4 and induces Wnt/PCP signaling via clathrin-mediated endocytosis to promote morphogenesis. *Dev. Cell* **20**, 303-314.

Ringelmann, B., Röder, C., Hallmann, R., Maley, M., Davies, M., Grounds, M., Sorokin, L. (1999). Expression of laminin α1, α2, α4, and α5 chains, fibronectin, and tenascin-C in skeletal muscle of dystrophic 129ReJdy/dyMice. *Exp. Cell Res.* **246**, 165-182.

Sabine, A., Agalarov, Y., Maby-El Hajjami, H., Jaquet, M., Hägerling, R., Pollmann, C., Bebber, D., Pfenniger, A., Miura, N., Dormond, O. et al. (2012). Mechanotransduction, PROX1, and FOXC2 cooperate to control connexin37 and calcineurin during lymphatic-valve formation. *Dev. Cell* **22**, 430-445.

Sabine, A., Bovay, E., Demir, C. S., Kimura, W., Jaquet, M., Agalarov, Y., Zangger, N., Scallan, J. P., Graber, W., Gulpinar, E. et al. (2015). FOXC2 and fluid shear stress stabilize postnatal lymphatic vasculature. *J. Clin. Invest.* **125**, 3861.

Sweet, D. T., Jiménez, J. M., Chang, J., Hess, P. R., Mericko-Ishizuka, P., Fu, J., Xia, L., Davies, P. F. and Kahn, M. L. (2015). Lymph flow regulates collecting lymphatic vessel maturation in vivo. *J. Clin. Invest.* **125**, 2995-3007.

Tatin, F., Taddei, A., Weston, A., Fuchs, E., Devenport, D., Tissir, F. and Makinen, T. (2013). Planar cell polarity protein Celsr1 regulates endothelial adherens junctions and directed cell rearrangements during valve morphogenesis. *Dev. Cell* **26**, 31-44.

Tzima, E., Irani-Tehrani, M., Kiosses, W. B., Dejana, E., Schultz, D. A., Engelhardt, B., Cao, G., DeLisser, H. and Schwartz, M. A. (2005). A mechanosensory complex that mediates the endothelial cell response to fluid shear stress. *Nature* **437**, 426-431.

Wang, Y., Guo, N. and Nathans, J. (2006). The role of Frizzled3 and Frizzled6 in neural tube closure and in the planar polarity of inner-ear sensory hair cells. *J. Neurosci.* **26**, 2147-2156.

Yin, H., Copley, C. O., Goodrich, L. V. and Deans, M. R. (2012). Comparison of phenotypes between different vangl2 mutants demonstrates dominant effects of the Looptail mutation during hair cell development. *PLoS ONE* **7**, e31988.

Supplementary figures

Fig. S1.

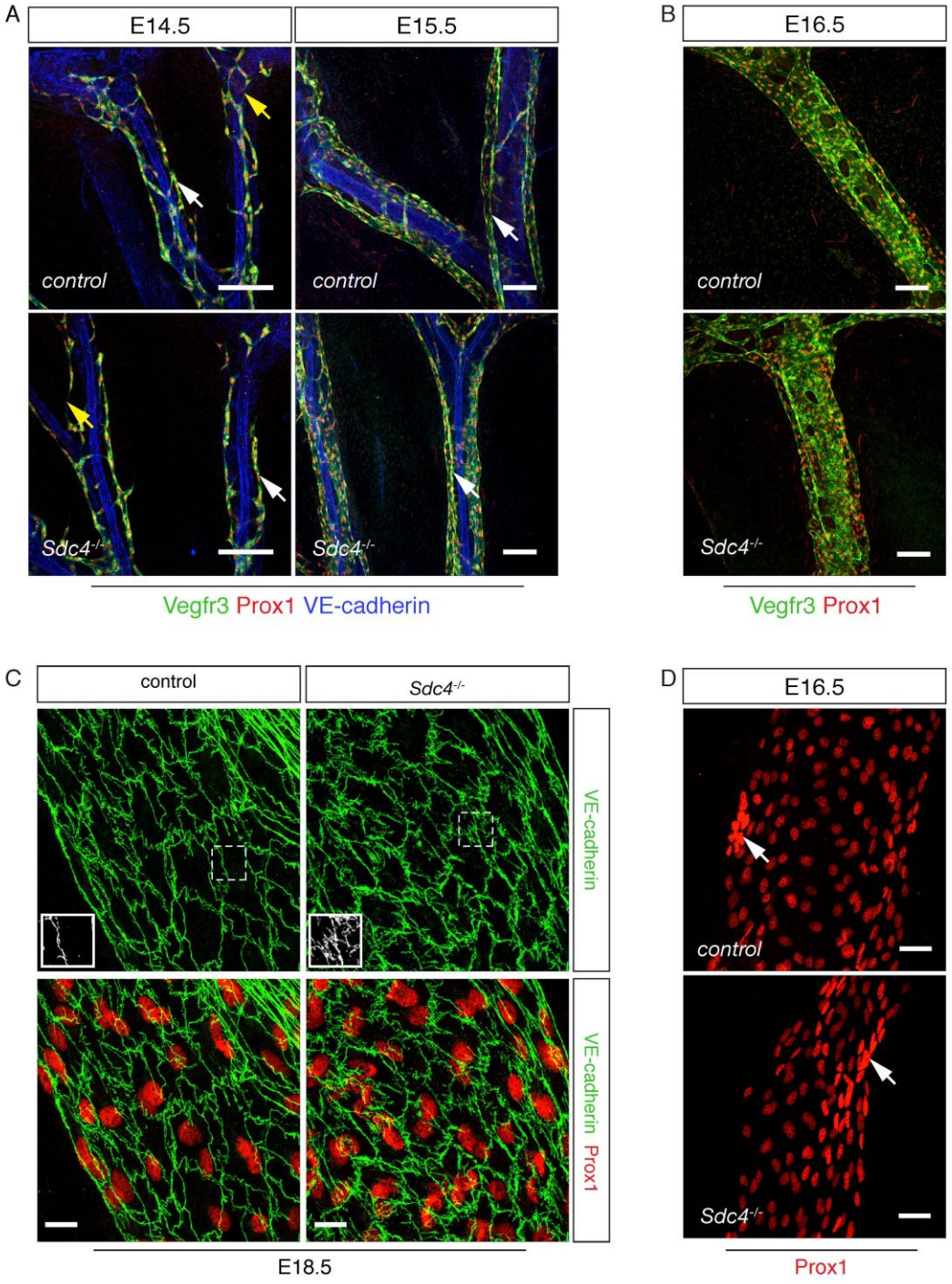

Fig. S1 The development of mesenteric lymphatic vessels in control and *Sdc4*$^{-/-}$ mice. **A,B:** Whole-mount antibody staining of mesenteric lymphatic vessels in control and *Sdc4* null mice at various developmental stages as indicated. Scale bars: 100um. **C:** Whole-mount immunofluorescence staining. LEC cell-cell junctions in *Sdc4* nulls are less linear compared with littermate controls. Inserts are enlarged images of boxed areas. Scale bars: 15um. **D:** Immunostaining for Prox1 showing a cluster of Prox1^{high} lymphatic-valve-forming ECs aligned along lymphatic vessel wall in control (arrow) and *Sdc4*$^{-/-}$ mice (arrow). Scale bars: 30um.

Fig. S2.

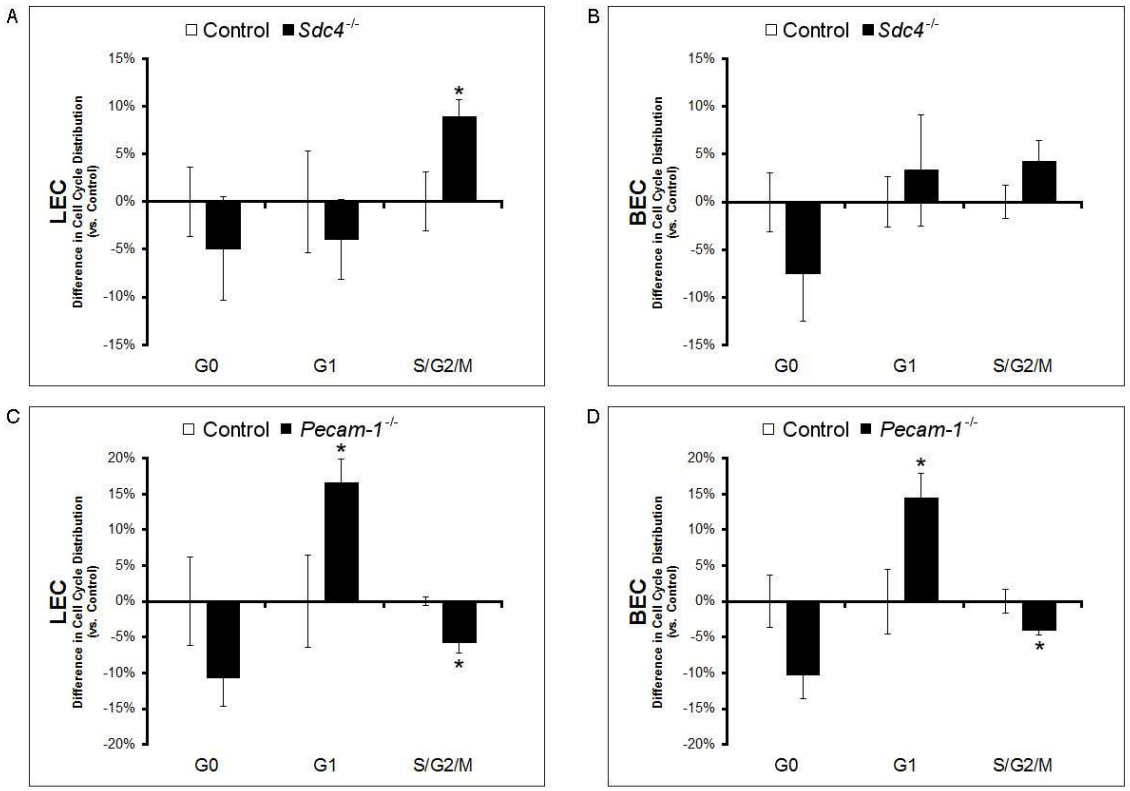

Fig. S2 Cell cycle distribution of LECs and BECs in *Sdc4*$^{-/-}$ and *Pecam-1*$^{-/-}$ mice.

A-D: Analysis of cell cycle distribution of LECs and BECs isolated from mesenteries of E18.5 WT, *Sdc4*$^{-/-}$ (A, B) or *Pecam-1*$^{-/-}$ (C, D) mice using FACS.

Fig. S3.

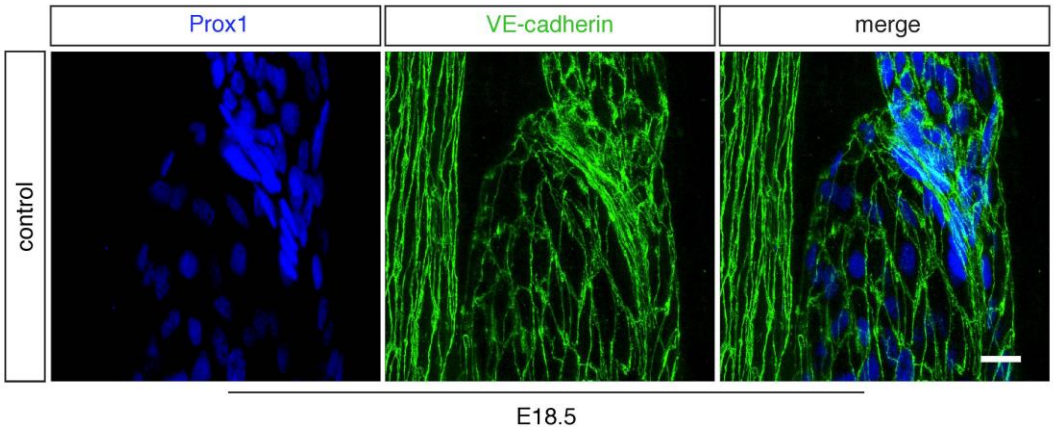

Fig. S3 The morphology and orientation of LECs are correlated with nuclear morphology and orientation. Immunofluorescence labeling for Prox1 (blue) and VE-cadherin (green) showing nuclear morphology and orientation of LECs are highly correlated with cell morphology and orientation in mesenteric lymphatic vessels in control mice. Scale bar: 15um.

Fig. S4.

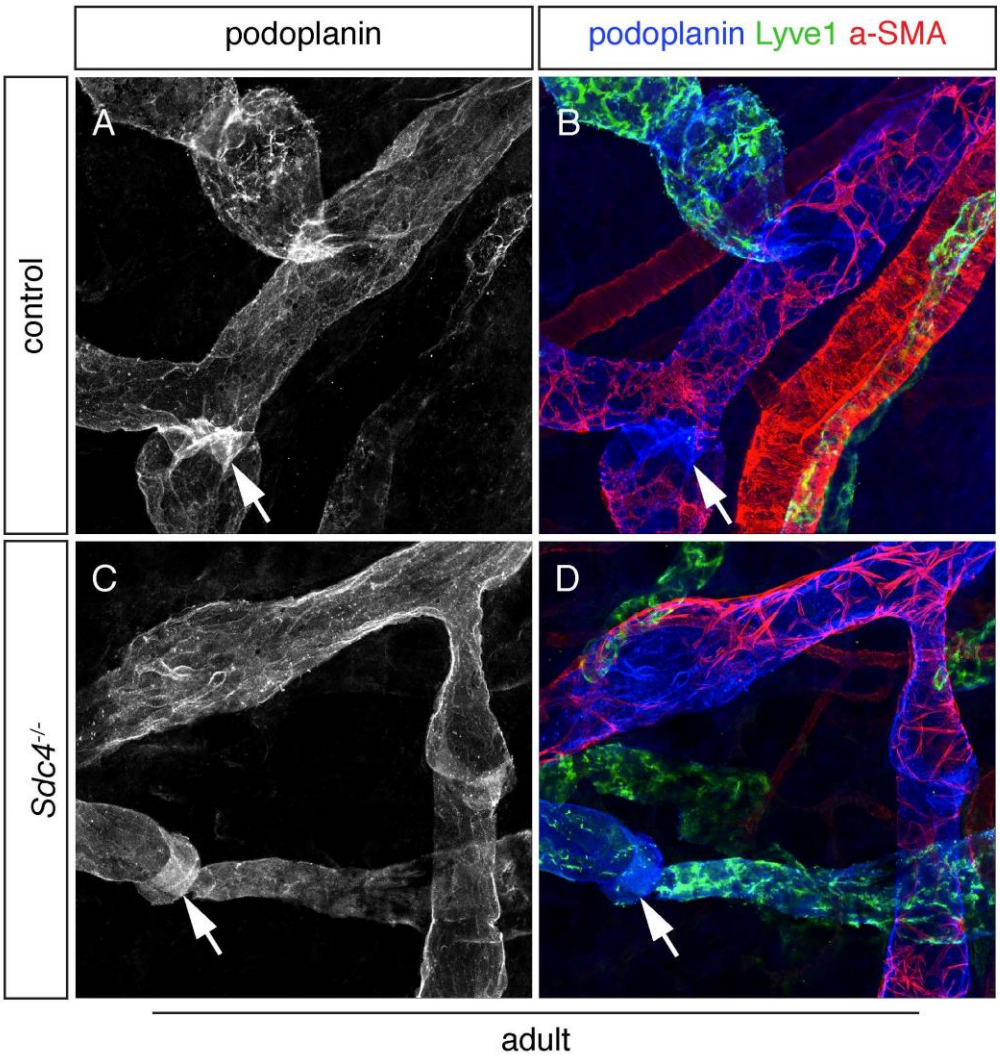

Fig. S4 Abnormal lymphatic valves are observed in *Sdc4* null adult mice. **A-D:** Whole-mount antibody staining of adult mouse ear skin. (A,B) Arrows indicate normal lymphatic valves formed in control mice. (C,D) Arrows indicate abnormal lymphatic valves in *Sdc4* nulls.

Fig. S5.

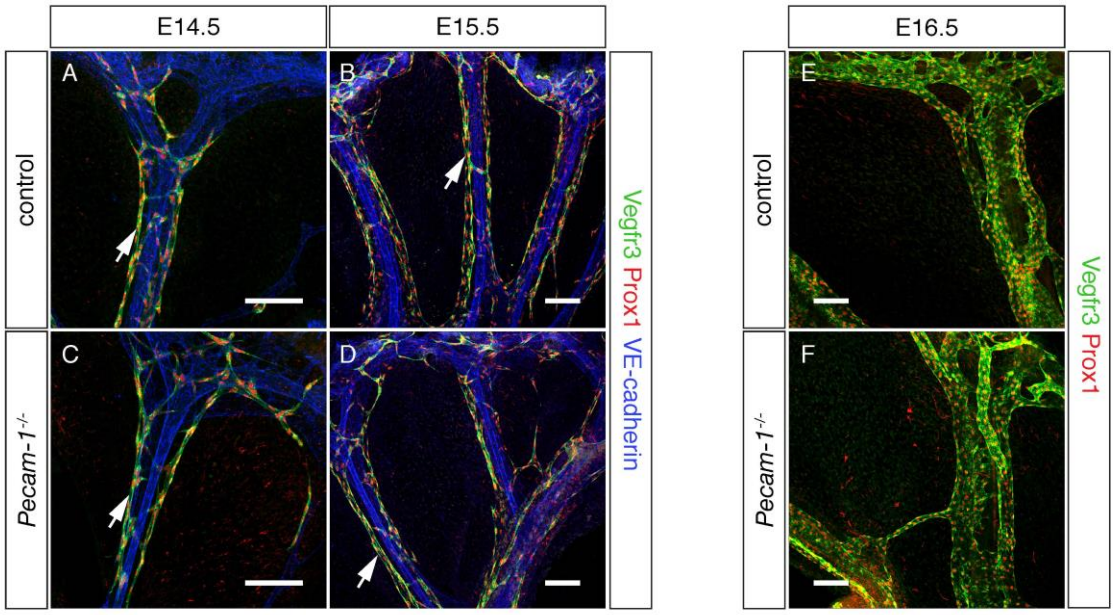

Fig. S5 Lymphatic vessels are developed normally in *Pecam-1*$^{-/-}$ mice from E14.5 to E16.5. **A-F:** Formation of mesenteric lymphatic vessels (Prox1+, Vegfr3+, VE-cadherin+) in *Pecam1*$^{-/-}$ mice (C, D, arrows, and F) is similar as in controls (A, B, arrows and E) from E14.5 to E16.5. Scale bars: 100um.

Fig. S6.

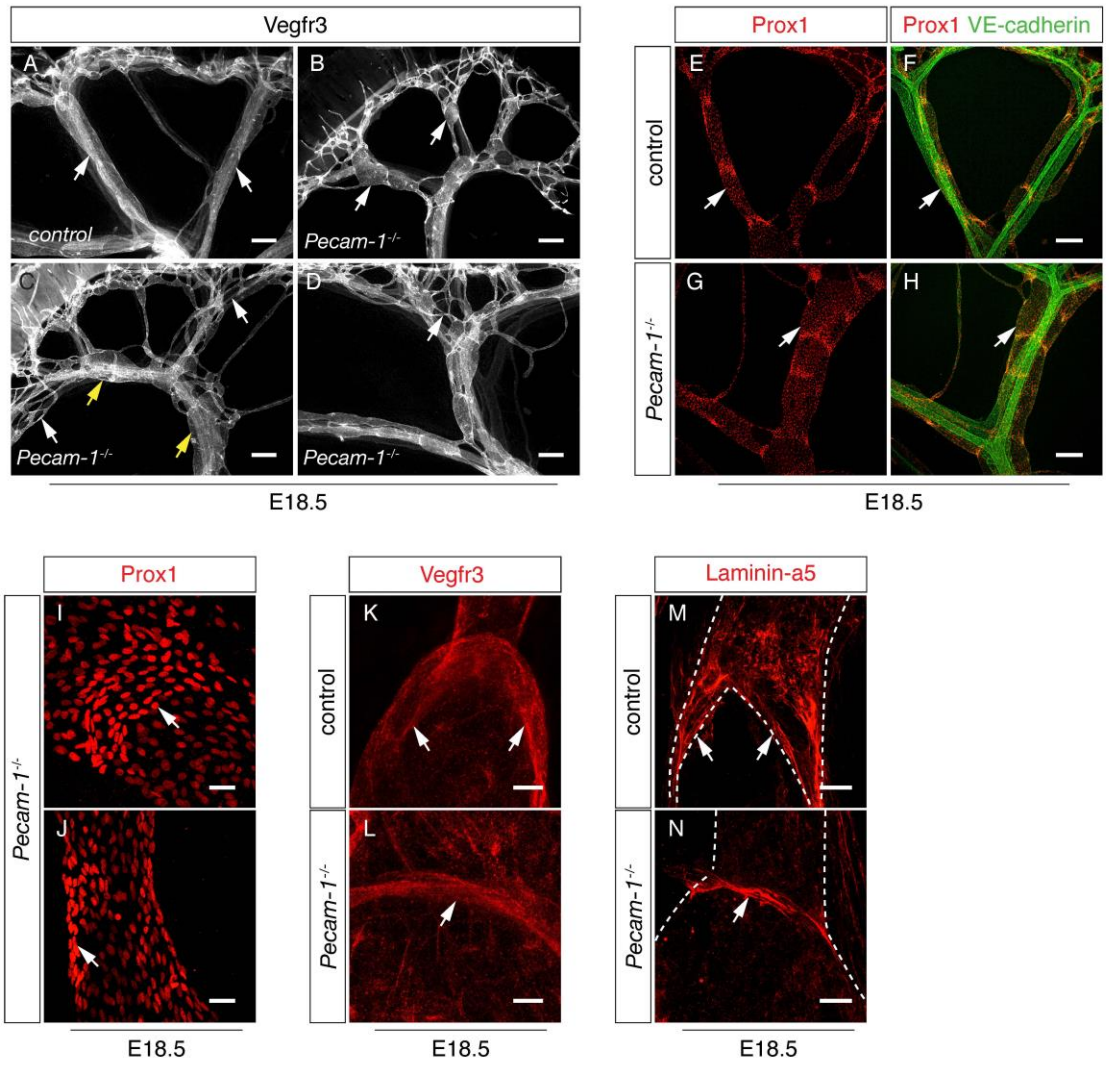

Fig. S6 *Pecam-1* null mice exhibit lymphatic remodeling defects at E18.5. **A-H:** Irregular (B, arrows), enlarged (C, yellow arrows, G, H, arrows) and abnormally branched (C, white arrows, D, arrow) mesenteric lymphatic vessels are developed in *Pecam-1* knockout mice at E18.5 but not in controls (A, E and F, arrows). Scale bars: 200um.

I-J: Antibody staining for Prox1 shows less elongated (I, arrow), loosely organized (I) nuclei of Prox1^{high} lymphatic-valve-forming ECs in *Pecam-1* null mice. Prox1^{high} valve-forming cells remained to the longitudinal axis of lymphatic vessels are observed in *Pecam-1* nulls at E18.5 (J, arrow). Scale bars: 30um. **K-N:** Ring-shape immature lymphatic valves developed in *Pecam-1*$^{-/-}$ animals (L, N, arrows). Leaflets of mature lymphatic valves in control mice (K, M, arrows). Scale bars: K-L, 10um; M-N, 15um.

Fig. S7.

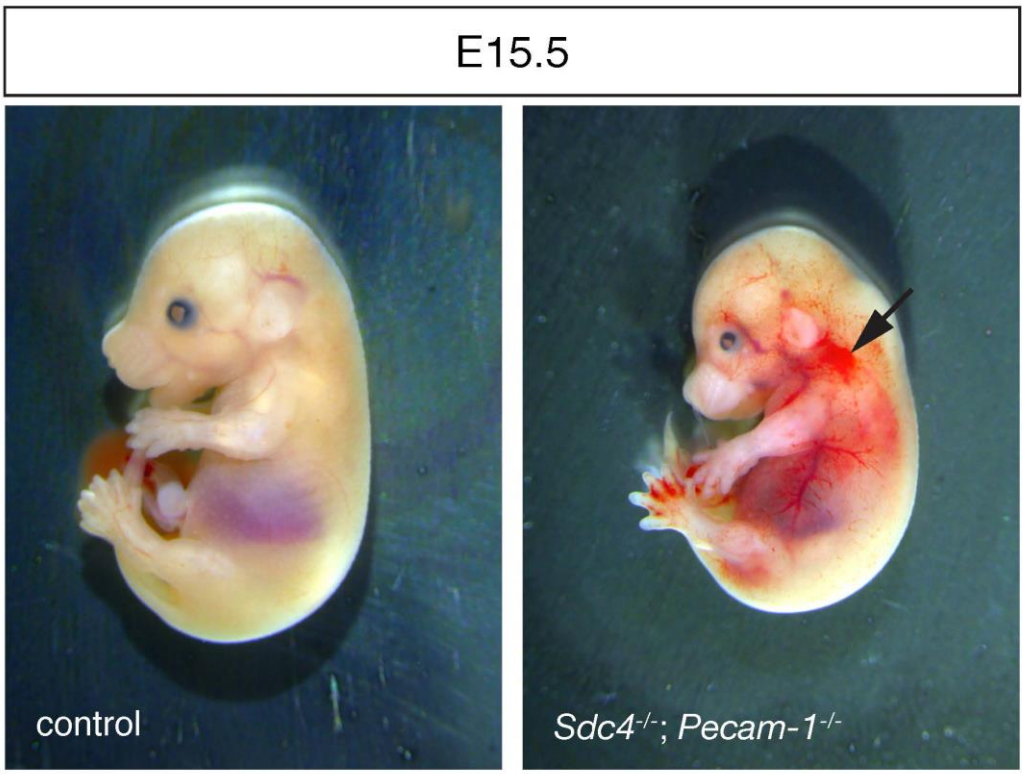

Fig. S7 Blood-filled jugular lymph sac is developed in *Sdc4*$^{-/-}$; *Pecam-1*$^{-/-}$ mouse. Grossly dissected control and *Sdc4*$^{-/-}$; *Pecam-1*$^{-/-}$ mouse embryos at E15.5. Arrow indicates blood-filled jugular lymph sac.

Fig. S8.

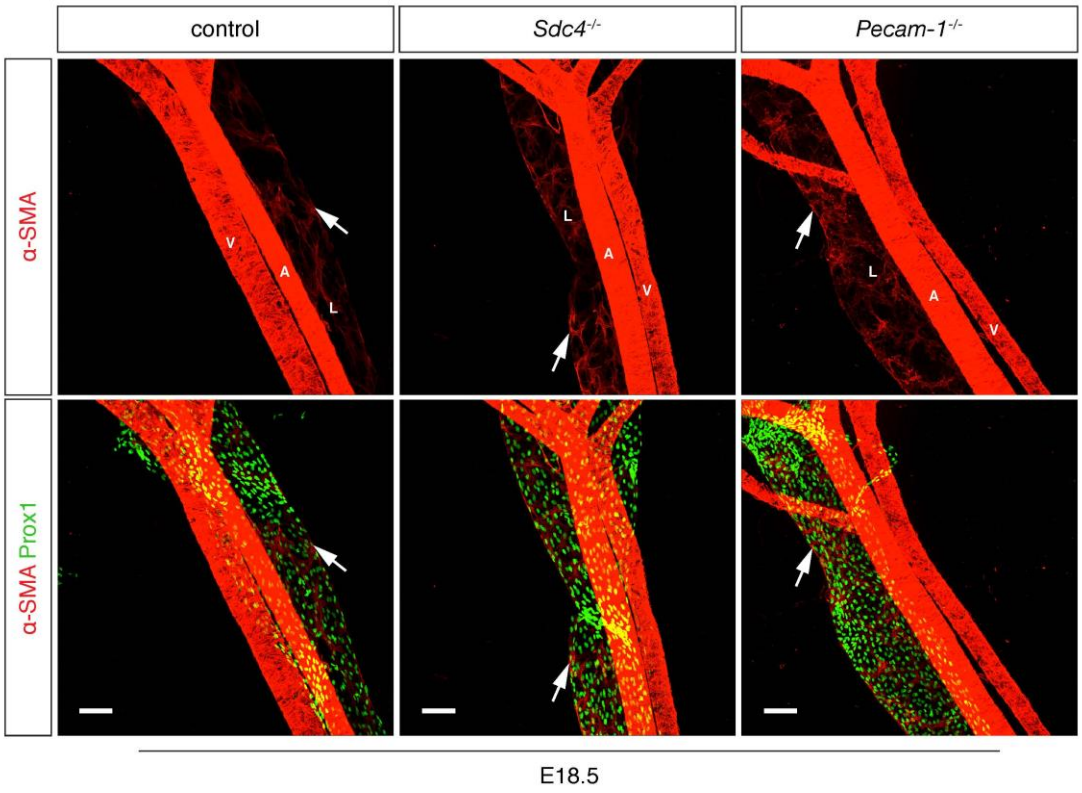

Fig. S8 Increased mural cell coverage in lymphatic vessels in *Sdc4*$^{-/-}$ or *Pecam-1*$^{-/-}$ mice. Mural cell (a-SMA+) recruitment in mesenteric lymphatic vessels in *Sdc4*$^{-/-}$ (arrows) or *Pecam-1*$^{-/-}$ (arrows) mice is increased compared to littermate controls (arrows). A=artery, V=vein, L=lymphatics. Scale bars: 100um.

Fig. S9.

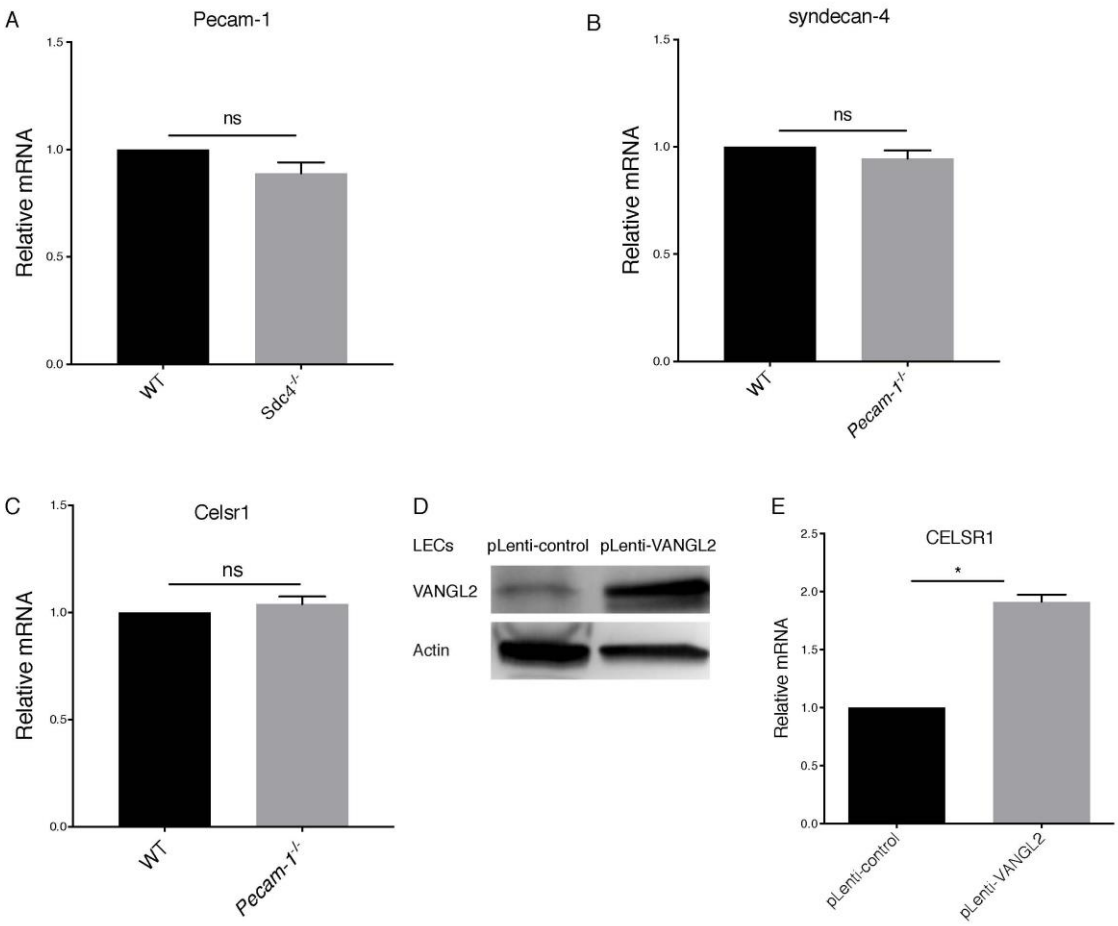

Fig. S9 qRT-PCR and western blotting analysis. **A-C:** qRT-PCR for various gene expression in thoracic duct of WT, *Sdc4*$^{-/-}$ or *Pecam-1*$^{-/-}$ mice. mRNA expression was normalized in relation to the expression of endogenous 18S rRNA. Mann-Whitney test (n = 4 (A, B), n=7 (C)). Values are mean ± SEM. **D:** Western blotting shows VANGL2 overexpression in LECs transduced with a lentivirus expressing VANGL2 (pLenti-VANGL2). **E:** qRT-PCR for CELSR1 expression in control LECs (pLenti-control) or cells overexpressing VANGL2 (pLenti-VANGL2). mRNA expression was normalized in

relation to the expression of endogenous β-actin. Mann-Whitney test (n = 4). Data represents mean ± SEM.

Fig. S10.

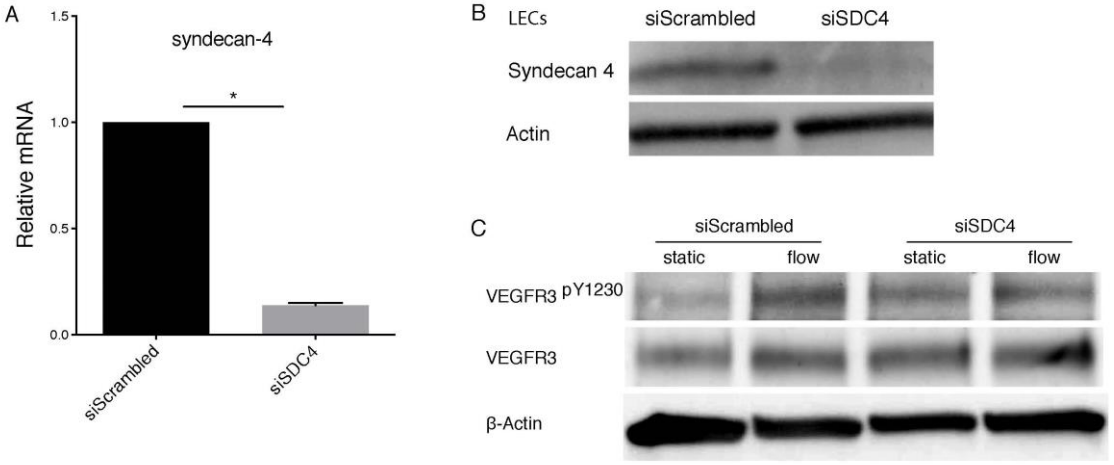

Fig. S10 Flow-induced activation of VEGFR3 signaling is reduced in *SDC4* KD LECs compared with controls. **A, B:** qRT-PCR (A) and western blotting (B) show reduced syndecan-4 expression in LECs transfected with siRNA against SDC4. mRNA expression was normalized in relation to the expression of endogenous β-actin. Mann-Whitney test (n = 4). Data are mean ± SEM. **C:** Western blotting shows flow-induced activation of VEGFR3 signaling.

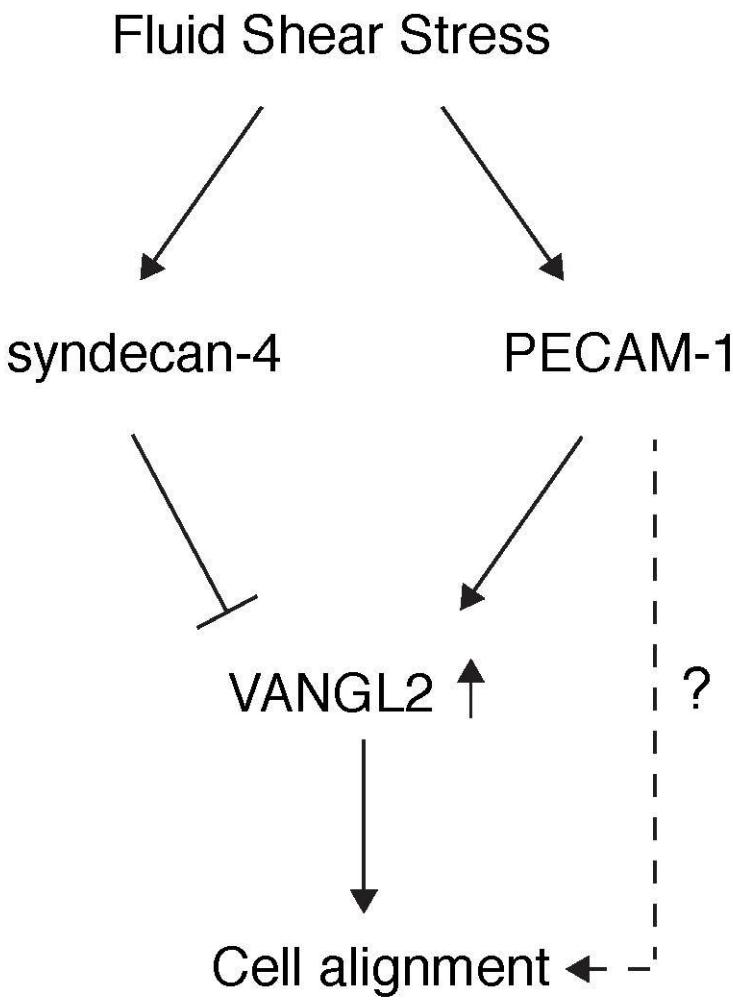

Fig. S11 A scheme illustrating syndecan-4 and PECAM-1 controlled flow signaling in LECs. Fluid shear stress transduced by the mechanosensory complex consisting PECAM-1/VE-cadherin/VEGFR2/3 up-regulates PCP protein VANGL2 in LEC. Syndecan-4-mediated flow signals ensures flow-induced VANGL2 expression within a certain range, which is critical for LECs to align to flow. In the absence of syndecan-4, flow-induced

VANGL2 expression are too high, cells fail to align. The mechanism of PECAM-1 controlled flow signaling in LECs remains unknown.